Table 3 Inhibition of electron transport enzymes by **1**

Enzyme	Complex	IC_{50} (μM)
NADH-fumarate reductase (*A. suum*)	I+II	5.1
NADH oxidase (bovine heart)	I+III+IV	19.8
NADH-rhodoquinone oxidoreductase (*A. suum* SMP)	I	23
Rhodoquinol-fumarate oxidoreductase (*A. suum* SMP)	II	35
NADH-ubiquinone oxidoreductase (bovine heart SMP)	I	16
Succinate-ubiquinone oxidoreductase (bovine heart SMP)	II	>100
Ubiquinol-cytochrome *c* oxidoreductase (bovine heart SMP)	III	20

Biological Activities of Paecilaminol

Though the *A. suum* NFRD inhibitory activity of **1** was moderate (IC_{50}=5.1 μM, Table 3), the inhibition was about 4 times more potent than that of bovine heart NADH oxidase (complexes I+III+IV). In the screening of NFRD inhibitors, we added 30 mg/ml of bovine serum albumin to the NFRD assay system to eliminate the effect of non-specific inhibition by fatty acids and acylglycerols. It is interesting that bovine serum albumin did not affect the NFRD inhibition of **1** (IC_{50}=3.2 μM). Generally, it reduced NFRD inhibition significantly. In the case of nafuredin, inhibition was reduced about 100-fold by bovine serum albumin.

We evaluated inhibitory activities of **1** against each complex using submitochondrial particles (SMP) of *A. suum* and bovine heart (Table 3). Compound **1** inhibited NADH-rhodoquinone oxidoreductase (complex I) and rhodoquinol-fumarate oxidoreductase (complex II) of *A. suum* SMP in similar concentration. It also inhibited NADH-ubiquinone oxidoreductase (complex I) and ubiquinol-cytochrome *c* oxidoreductase (complex III) of bovine heart SMP in similar concentration. However, the inhibition against bovine succinate-ubiquinone oxidoreductase (complex II) was weak. Therefore, **1** showed similar inhibitory activities against complexes I, II, and III of *A. suum* and bovine heart, except bovine complex II. It is not common for electron transport inhibitors to show such low selectivity. The only group that shows such wide inhibitions are the 2-alkyl-4,6-dinitrophenols, but their inhibitory activity against complex II is also weaker than that for complexes I and III [9]. The low selectivity of **1** may be due to its linear structure, because both amino and hydroxyl groups can freely rotate and be attached to enzymes.

Compound **1** is an amino alcohol, and its structure is similar to sphingosine (**2**), a long-chain base of sphingolipids. However, NFRD inhibition of **2** was very weak (Table 4). Fumonisin B_1 (**3**) [10], a fungal amino alcohol, did not inhibit NFRD at 100 μM. A simple alcohol 2-decanol also showed no inhibition against NFRD at 100 μM.

Table 4 NFRD inhibition by compounds related to **1**

Enzyme	IC_{50} (μM)
Sphingosine (**2**)	28
Fumonisin B_1 (**3**)	>100
2-Decanol	>100

Table 5 Antimicrobial activity of **1**

Microorganisms	MIC (μg/ml)
Staphylococcus aureus ATCC6538P	12.5
Bacillus subtilis ATCC6633	6.25
Micrococcus luteus ATCC9341	6.25
Mycobacterium smegmatis ATCC607	25
Escherichia coli NIHJ	>100
Escherichia coli IFO12734	>100
Pseudomonas aeruginosa IFO3080	>100
Xanthomonas campestris pv. *oryzae* KB88	>100
Candida albicans KF1	>100
Saccharomyces cerevisiae KF26	>100
Aspergillus niger ATCC6275	100
Mucor racemosus IFO4581	100

Nematocidal and insecticidal activities of **1** were studied by a microplate assay using free-living nematode *Caenorhabditis elegans* and brine shrimp *Artemia salina*. Minimum growth inhibitory concentrations of **1** against *C. elegans* and *A. salina* were 20 μg/ml and 5 μg/ml, respectively. As shown in Table 5, it exhibited moderate antimicrobial activity against Gram-positive bacteria.

Though **2** is a 2-aminoalkene with 1,3-diol residues, **1**

lacks 1-hydroxyl residue. Such 2-amino-3-alkanols or 2-amino-3-alkenols have been isolated from natural origins. Most of them were obtained from marine sponges, such as xestoaminols A~C isolated from *Xestospongia* sp. [11] and oceanapiside (**4**) isolated from *Oceanapia phillipensis* [12]. Xestoaminol A (**5**) showed nematocidal, antibacterial, and antifungal activity and inhibited reverse transcriptase [11]. Compound **4** showed antifungal activity [12]. It also exhibits inhibitory activity against a mycobacterial detoxification enzyme, mycothiol-*S*-conjugate amidase [13]. ES-285 (spisulosine 285, **6**) was isolated from the clam *Mactromeris polynyma*, and it disrupts the cytoskeleton of cancer cells [14]. Compound **6** may decrease the activity of the GTP-binding protein Rho. It is currently being evaluated in phase I clinical trials for advanced solid tumors. Fumonisins are fungal 2-amino-3-alkanols produced by *Fusarium verticillioides*. They are toxic and carcinogenic for animals and humans as a contaminant of grains [10, 15]. The analogous compounds, AAL toxins (AAL Toxin TA1=**7**), are 1-amino-2-alkanols and produced by the phytopathogenic fungus *Alternaria alternata* f. sp. *lycopersici* [16]. Both mycotoxins inhibit ceramide synthase (sphingosine *N*-acyltransferase) [15, 17]. Myriocin (ISP-I, **8**) is a 2-aminoalkan-1,3-diol compound produced by fungi, *Myriococcum albomyces* and *Isaria sinclairii* [18, 19]. It is a potent immunosuppressant inhibiting serine palmitoyltransferase, the enzyme that catalyzes the first step of sphingolipid biosynthesis [19, 20]. The derivative of **8**, FTY720, is in phase II clinical trials as an immunosuppressant [21].

As described above, amino alcohols have various biological activities. However, only a few have been reported to have an effect on electron transport enzymes. Galactosylsphingosine (psychosine), glucosylsphingosine, and **2** showed more than 50% inhibition against complex IV (cytochrome *c* oxidase) at 5 μM [22]. Though 3% of bovine serum albumin did not affect the NFRD inhibition of **1**, 1% of human serum albumin completely abolished complex IV inhibition of **2** and its glycosides [22]. As for complex I, *N*-acetylsphingosine and *N*-palmitoyl-sphingosine were reported to inhibit the enzyme [23]. However, the inhibition was weak (IC_{50}=20~40 μM), which is comparable with the NFRD inhibition of **2**. Therefore, **1** is the first amino alcohol that has NFRD inhibitory activity.

Experimental

General

NMR spectra were recorded on a Varian Inova 600 spectrometer ($^{2\text{-}3}J_{CH}$=8 Hz in HMBC). Chemical shifts are shown in δ values (ppm) relative to $CDCl_3$ at 7.26 ppm for ^{1}H NMR and at 77.0 ppm for ^{13}C NMR. Mass spectrometry was conducted on a JEOL JMS-AX505 HA spectrometer. The UV and IR spectra were measured with a Shimadzu UV-240 spectrophotometer and a Horiba FT-210 Fourier transform infrared spectrometer, respectively. Optical rotations were recorded on a JASCO model DIP-181 polarimeter.

Taxonomic Studies of the Producing Organism

Morphological observations of the paecilaminol producing strain were carried out using an Olympus Vanox-S AH-2 microscope and a JEOL JSM-5600 scanning electron microscope.

Media

The seed medium consisted of glucose 2.0%, Polypepton (Nihon Pharmaceutical Co.) 0.5%, yeast extract (Oriental Yeast Co.) 0.2%, KH_2PO_4 0.1%, $MgSO_4 \cdot 7H_2O$ 0.05%, and agar 0.1%, pH 5.7. The production medium consisted of glycerol 2.0%, sucrose 1.0%, ammonium acetate 0.5%, KH_2PO_4 0.1%, $MgSO_4 \cdot 7H_2O$ 0.05%, KCl 0.05%, Cultivater #100 (fish extract, Yaizu Suisankagaku Industry Co.) 0.2%, and agar 0.1%, pH 6.0.

Biological Studies

NFRD activity was measured as described previously [24]. The other enzyme assays were performed as described previously [4]. The assay method for nematocidal and insecticidal activities was reported previously [25]. The antimicrobial activity was measured by agar dilution method.

Acknowledgements We are grateful to Dr. Achim Harder of Bayer HealthCare AG, Animal Health-Research & Development-Parasiticides for valuable discussions. We also thank Ms. Akiko Nakagawa and Ms. Chikako Sakabe of School of Pharmaceutical Sciences, Kitasato University for measurements of mass spectra. This work was supported by a Grant-in-Aid for Scientific Research (14593006 to K.S. and 13854011 to K.K.) and a Grant-in-Aid for Encouragement of Young Scientists (12771373 to H.U.). This work was also supported in part by the Grant of the 21st Century COE Program, Ministry of Education, Culture, Sports, Science, and Technology.

References

1. Shiomi K, Ōmura S. Antiparasitic agents produced by microorganisms. Proc Jpn Acad, Ser B 80: 245–258 (2004)
2. Komuniecki R, Tielens AGM. Carbohydrate and energy

metabolism in parasitic helminths. *In* Molecular Medical Parasitology. *Ed.* J. J. Marr, *et al.*, pp. 339–358. Academic Press, London (2003)
3. Kita K, Nihei C, Tomitsuka E. Parasite mitochondria as drug target: diversity and dynamic changes during the life cycle. Curr Med Chem 10: 2535–2548 (2003)
4. Ōmura S, Miyadera H, Ui H, Shiomi K, Yamaguchi Y, Masuma R, Nagamitsu T, Takano D, Sunazuka T, Harder A, Kölbl H, Namikoshi M. Miyoshi H, Sakamoto K, Kita K. An anthelmintic compound, nafuredin, shows selective inhibition of complex I in helminth mitochondria. Proc Natl Acad Sci USA 98: 60–62 (2001)
5. Ui H, Shiomi K, Yamaguchi Y, Masuma R, Nagamitsu T, Takano D, Sunazuka T, Namikoshi M, Ōmura S. Nafuredin, a novel inhibitor of NADH-fumarate reductase, produced by *Aspergillus niger* FT-0554. J Antibiot 54: 234–238 (2001)
6. Miyadera H, Shiomi K, Ui H, Yamaguchi Y, Masuma R, Tomoda H, Miyoshi H, Osanai A, Kita K, Ōmura S. Atpenins, potent and specific inhibitors of mitochondrial complex II (succinate-ubiquinone oxidoreductase). Proc Natl Acad Sci USA 100: 473–477 (2003)
7. Ōmura S, Shiomi K, Masuma R. (The Kitasato Institute). Novel substance FKI-0550 manufacture with *Paecilomyces*. PCT Int Appl, WO 2003048373, June 12 (2003)
8. Uhlig S, Petersen D, Flåøyen A, Wilkins A. 2-Amino-14,16-dimethyloctadecan-3-ol, a new sphingosine analogue toxin in the fungal genus *Fusarium*. Toxicon 46: 513–522 (2005)
9. Tan AK, Ramsay RR, Singer TP, Miyoshi H. Comparison of the structures of the quinone-binding sites in beef heart mitochondria. J Biol Chem 268: 19328–19333 (1993)
10. Gelderblom WCA, Jaskiewicz K, Marasas WFO, Thiel PG, Horak RM, Vleggaar R, Kriek NPJ. Fumonisins-novel mycotoxins with cancer-promoting activity produced by *Fusarium moniliforme*. Appl Envir Microbiol 54: 1806–1811 (1988)
11. Jiménez C, Crews P. Novel marine sponge amino acids, 10. Xestoaminols from *Xestospongia* sp. J Nat Prod 53: 978–982 (1990)
12. Nicholas GM, Hong TW, Molinski TF, Lerch ML, Cancilla MT, Lebrilla CB. Oceanapiside, an antifungal bis-α,ω-amino alcohol glycoside from the marine sponge *Oceanapia phillipensis*. J Nat Prod 62: 1678–1681 (1999)
13. Nicholas GM, Eckman LL, Newton GL, Fahey RC, Ray S, Bewley CA. Inhibition and kinetics of *Mycobacterium tuberculosis* and *Mycobacterium smegmatis* mycothiol-*S*-conjugate amidase by natural product inhibitors. Bioorg Med Chem 11: 601–608 (2003)
14. Cuadros R, Montejo de Garcini E, Wandosell F, Faircloth G, Fernandez-Sousa JM, Avila J. The marine compound spisulosine, an inhibitor of cell proliferation, promotes the disassembly of actin stress fibers. Cancer Lett 152: 23–29 (2000)
15. Merrill AH Jr, Wang E, Gilchrist DG, Riley RT. Fumonisins and other inhibitors of *de novo* sphingolipid biosynthesis. *In* Advances in Lipid Research Vol. 26. Sphingolipids. Part B: Regulation and Function of Metabolism. *Ed.* R. M. Bell, *et al.*, pp. 215–234. Academic Press, San Diego (1993)
16. Bottini AT, Bowen JR, Gilchrist DG. Phytotoxins. II. Characterization of a phytotoxic fraction from *Alternaria alternata* f. sp. *lycopersici*. Tetrahedron Lett 22: 2723–2726 (1981)
17. Desai K, Sullards MC, Allegood J, Wang E, Schmelz EM, Hartl M, Humpf H-U, Liotta DC, Peng Q, Merrill AH Jr. Fumonisins and fumonisin analogs as inhibitors of ceramide synthase and inducers of apoptosis. Biochim Biophy Acta 1585: 188–192 (2002)
18. Kluepfel D, Bagli J, Baker H, Charest MP, Kudelski A, Sehgal SN, Vezina C. Myriocin, a new antifungal antibiotic from *Myriococcum albomyces*. J. Antibiot 25: 109–115 (1972)
19. Fujita T, Inoue K, Yamamoto S, Ikumoto T, Sasaki S, Toyama R, Chiba K, Hoshino Y, Okumoto T. Fungal metabolites. Part 11. A potent immunosuppressive activity found in *Isaria sinclairii* metabolite. J. Antibiot 47: 208–215 (1994)
20. Miyake Y, Kozutsumi Y, Nakamura S, Fujita T, Kawasaki T. Serine palmitoyltransferase is the primary target of a sphingosine-like immunosuppressant, ISP-1/myriocin. Biochem Biophys Res Commun 211: 396–403 (1995)
21. Tedesco-Silva H, Mourad G, Kahan BD, Boira JG, Weimar W, Mulgaonkar S, Nashan B, Madsen S, Charpentier B, Pellet P, Vanrenterghem Y. FTY720, a novel immunomodulator: efficacy and safety results from the first phase 2A study in *de novo* renal transplantation. Transplantation 77: 1826–1833 (2004)
22. Igisu H, Hamasaki N, Ito A, Ou W. Inhibition of cytochrome *c* oxidase and hemolysis caused by lysosphingolipids. Lipids 23: 345–348 (1988)
23. Di Paola M, Cocco T, Lorusso M. Ceramide interaction with the respiratory chain of heart mitochondria. Biochemistry 39: 6660–6668 (2000)
24. Shiomi K, Ui H, Suzuki H, Hatano H, Nagamitsu T, Takano D, Miyadera H, Yamashita T, Kita K, Miyoshi H, Harder A, Tomoda H, Ōmura S. A γ-lactone form nafuredin, nafuredin-γ, also inhibits helminth complex I. J Antibiot 58: 50–55 (2005)
25. Enomoto Y, Shiomi K, Matsumoto A, Takahashi Y, Iwai Y, Harder A, Kölbl H, Woodruff HB, Ōmura S. Isolation of a new antibiotic oligomycin G produced by *Streptomyces* sp. WK-6150. J Antibiot 54: 308–313 (2001)

J. Biochem. **139**, 373–381 (2006)
doi:10.1093/jb/mvj040

Up-Regulation of Heme Biosynthesis during Differentiation of Neuro2a Cells

Noriko Shinjyo and Kiyoshi Kita*
Department of Biomedical Chemistry, Graduate School of Medicine, The University of Tokyo, 7-3-1 Hongo, Bunkyo-ku, Tokyo 113-0033

Received October 10, 2005; accepted December 12, 2005

Heme is an iron-containing tetrapyrrole molecule that functions as a prosthetic group for proteins such as mitochondrial respiratory enzymes. Several studies have suggested that heme has essential functions in the construction and maintenance of the nervous system. In this study, the contents of three biologically important forms of heme (types *a*, *b*, and *c*) and the expression of heme biosynthetic enzymes were examined in differentiating Neuro2a cells. During neuronal differentiation, there were increases in the cellular heme levels and increases in the mRNA levels for the rate-limiting enzymes of heme biosynthesis, such as aminolevulinic acid synthase (ALAS; EC 2.3.1.37) and coproporphyrinogen oxidase (EC 1.3.3.3). With respect to heme contents, heme *b* increased in the late phase of differentiation, but no apparent increase in heme *a* or *b* was observed in the early phase. In contrast, heme *c* (cytochrome *c*) markedly increased during the early phase of differentiation. This change preceded the increase in heme *b* and the up-regulation of the mRNA levels for heme biosynthetic enzymes. This study suggests the up-regulation of heme biosynthesis and differential regulation of the heme *a*, *b*, and *c* levels during neuronal differentiation.

Key words: cytochrome *c*, differentiation, heme, mitochondria, neuron.

Abbreviations: ALAS, 5-aminolevulinic acid synthase; USP, upstream primer; DSP, downstream primer.

Heme is an essential prosthetic group of mitochondrial respiratory enzymes and globin proteins, and several proteins are known to have regulatory heme-binding domains (*1*, *2*). Heme is required for the construction and maintenance of the nervous system, and altered heme metabolism is observed in patients with Alzheimer's disease. In particular, mitochondrial cytochrome *c* oxidase (complex IV; EC 1.9.3.1), which is a heme-containing enzyme, is markedly reduced in Alzheimer's disease (*3–6*). Heme has been shown to inhibit the *in vitro* aggregation of amyloid β protein and to protect neuronal cells from its toxic effects (*7*). Also, some heme proteins, such as neuroglobin and neuronal nitric oxide synthase (EC 1.14.13.39) are highly expressed in neuronal cells, and heme appears to be essential for their growth (*8*, *9*). In fact, the addition of heme to the culture medium induces the differentiation of neuroblastoma cells (*10*), and neuronal differentiation does not proceed when precursor cells are exposed to succinyl-acetone, an inhibitor of heme biosynthesis (*11–13*). Collectively, these studies indicate that heme is essential for the function of neurons. However, how heme synthesis is regulated during the course of neurogenesis has not been determined.

There are three biologically important types of heme, types *a*, *b* and *c* (Fig. 2b), which differ in their porphyrin ring structures (*14*). Heme *b* is the product of ferrochelatase (EC 4.99.1.1), the terminal enzyme of the heme synthetic pathway, whereas hemes *a* and *c* are formed through modification of heme *b*. Heme *b*, the most common form of heme, is the prosthetic group of proteins such as globins and is also present in mitochondrial respiratory complexes. Heme *c* differs from heme *b* (or protoheme) in that its two vinyl side chains are covalently bound to the protein itself. Examples of proteins containing a *c*-type heme include cytochromes *c* and c_1. In contrast to that of heme *b*, the methyl side chain of heme *a* is oxidized into a formyl group, and one of the vinyl side chains (on C2) is replaced by an isoprenoid (farnesyl) chain. The only known protein to contain heme *a* is complex IV of the mitochondrial respiratory system, which contains two noncovalently bound heme *a* groups. All three forms of heme are essential components of the mitochondrial respiratory system and a variety of other systems, such those regarding gas transport and storage by globins.

In this study, we analyzed the expression of mRNAs for heme synthetic enzymes during retinoic acid-induced differentiation of Neuro2a cells. We also examined the alteration in the contents of the three types of heme (*a*, *b*, and *c*) in these cells.

MATERIALS AND METHODS

Cell Culture—Neuro2a cells were cultured in Dulbecco's modified Eagle's medium (Sigma-Aldrich, St. Louis, MO, USA) supplemented with 10% (v/v) fetal bovine serum (Gibco BRL Life Technologies, Paisley, Scotland), 100 U/ml penicillin, 100 μg/ml streptomycin, and 292 μg/ml glutamine at 37°C in a humidified 5% (v/v) CO_2 incubator. The cells were seeded at 1.0×10^6 and then incubated for 24 h in 90-mm-diameter plastic dishes. Then induction of

*To whom correspondence should be addressed. Tel: +81-3-5841-3526, Fax: +81-3-5841-3444, E-mail: kitak@m.u-tokyo.ac.jp

differentiation was performed as described (*15–17*). Cells were differentiated with 20 μM retinoic acid in Dulbecco's modified Eagle's medium containing 2% (v/v) fetal bovine serum for 0–96 h (0 h means untreated control, cultured without retinoic acid). The culture medium was routinely changed every 2 days.

Quantitative Real-Time PCR—Total RNA was isolated from cells using TRIZOL reagent (Invitrogen, Carlsbad, CA, USA) following the manufacturer's protocol. RNA was reverse-transcribed, and complementary DNAs were synthesized using an oligo (dT) primer. Real-time PCR was performed using a LC real-time PCR apparatus (Roche Diagnostics, Mannheim, Germany) and a Quantitect SYBR-Green RT-PCR Kit (Qiagen, Hilden, Germany) in a 20 μl volume containing 0.5 μM of each upstream primer (USP) and downstream primer (DSP) according to the manufacturer's instructions. The primers used were as follows: β-actin-USP, 5′-tggaatcctgtggcatccatgaaac-3′; β-actin-DSP, 5′-taaaacgcagctcagtaacagtccg-3′; ferrochelatase-USP, 5′-ccactgtccacaaagtc-3′; ferrochelatase-DSP, 5′-gatagcctcatctgtctg-3′; ALAS-1-USP, 5′-gtcaagcttctgaggc-3′; ALAS-1-DSP, 5′-cctggtcatcaactc-3′; 5-aminolevulinic acid dehydratase (EC 4.2.1.24)-USP, 5′-ggtgaagccgggattgc-3′; 5-aminolevulinic acid dehydratase-DSP, 5′-ggaaggccgtcatggt-3′; porphobilinogen deaminase (EC 2.5.1.61,)-USP, 5′-ccgtagcagtgcatacagtg-3′; porphobilinogen deaminase-USP, 5′-ctggatggtggcctgcatag-3′; protoporphyrinogen oxidase (EC 1.3.3.4)-USP, 5′-ccattccagcttcagagc-3′; protoporphyrinogen oxidase-DSP, 5′-cagacaagctcctcggtac-3′; coproporphyrinogen oxidase (EC 1.3.3.3)-USP, 5′-ctccaggatccaggatc-3′; coproporphyrinogen oxidase-DSP, 5′-cctttggatggcgcaac-3′; uroporphyrinogen cosynthase (EC 4.2.1.75)-USP, 5′-ctatcagacagttcc-3′; uroporphyrinogen cosynthase-DSP, 5′-cgcctgaatatactc-3′; uroporphyrinogen decarboxylase (EC 4.1.1.37)-USP, 5′-ggctatgaggtagttggac-3′; and uroporphyrinogen decarboxylase-DSP, 5′-gatgcatacaaggcacagg-3′. The PCR was carried out as follows: initial denaturation at 95°C for 10 min, followed by 40 cycles of 10 s at 95°C, 10 s at 60°C, and 20 s at 72°C. The mRNA levels were normalized as to the level of β-actin mRNA.

Extraction and Separation of Hemes—Extraction and separation of hemes were performed as described previously (*18*) with slight modifications. Cells and mitochondria were solubilized with 1% (v/v) Tween20 and then hemes were extracted with acetone containing 2.5% (v/v) HCl. The mixture was vortexed, centrifuged for 5 min at 1,400 × *g* and then mixed with 50% (v/v) acetonitrile. Insoluble material was removed by a second centrifugation. Next, the extracts were adjusted to approximately pH 3.5 with 1.65 M ammonium hydroxide and then clarified by centrifugation. The extracts were applied to a 2 × 50 mm Luna 3 micron C18(2) column (Phenomenex, CA, Torrance, USA). Hemes were eluted at the flow rate of 0.2 ml/min using a gradient of 10–50% (v/v) acetonitrile for the first 1 ml, followed by a linear gradient of 50–75% (v/v) acetonitrile for the subsequent 1 ml. All gradient solutions contained 0.05% (v/v) trifluoroacetic acid. The elution and identification of heme compounds were performed at 400 nm. Heme *b* standard was purchased from Sigma. Heme-*a* was prepared from partially purified complex IV from bovine heart mitochondria (*19*) and used as a standard. Hemes *a* and *b* were quantified by comparing each peak area with that of a known amount of the standard. Data are shown as concentrations of heme per mg protein.

Sodium Dodecyl Sulphate–Polyacrylamide Gel Electrophoresis (SDS-PAGE) and Heme/Protein Staining—Mitochondria were prepared using an ApoAlert cell fractionation kit (BD Biosciences, CA, USA) following the protocol in the user manual. The isolated mitochondria were incubated for 15 min at 42°C in 124 mM Tris, pH 7.0, 20% (v/v) glycerol, and 4.6% (w/v) SDS, but without β-mercaptoethanol. Proteins were separated by electrophoresis on 10–20% (w/v) polyacrylamide gradient gels (Daiichi, Tokyo, Japan) and then transferred to nitrocellulose filters (BA 85 Schleicher & Schuell, Dassel, Germany) as described by Towbin *et al.* (*20*).

To determine the content of heme *c*, the detection procedure for *c*-type cytochrome, which is based on the intrinsic peroxidase activity of the heme groups of denatured *c*-type cytochromes, reported by Vargas *et al.* (*21*) was used. *C*-type cytochromes, denatured and separated by SDS-PAGE, were detected directly using an enhanced chemiluminescence (ECL) system (Amersham Biosciences, Piscataway, NJ, USA) according to the manufacturer's instructions.

After protein transfer, the nitrocellulose membranes were further used for the detection of cytochrome *c* and VDAC proteins with antibodies as mentioned below. Detection of proteins by means of Western blotting was performed as follows: after blocking with 5% (w/v) skim milk in Tris-buffered saline plus Tween 20 [TBST: 50 mM Tris, pH 7.5, 0.15 M NaCl, 0.05% (w/v) Tween 20], the membranes were incubated with primary antibodies in TBST containing 2% (w/v) skim milk, after which they were incubated with secondary antibodies in TBST containing 2% (w/v) skim milk. Detection was carried out with an alkaline phosphatase system. Densitometric intensity was quantified with NIH image 1.62.

To determine the cytochrome *c* content of whole cells, total cell lysates were prepared by washing the cells twice with phosphate-buffered saline and then homogenizing them in cooled lysis buffer (10 mM EDTA, 1% Tween20, 10 mM Tris-HCl, pH 7.5) supplemented with a protease inhibitor cocktail for general use (Sigma-Aldrich). After centrifugation to remove insoluble material, equivalent amounts of protein were denatured in sample buffer [60.5 mM Tris-HCl, pH 6.8, 2% (w/v) SDS, 5% (v/v) β-mercaptoethanol, 7.9% (v/v) glycerol, 0.05% (w/v) bromophenol blue] and then heated at 94°C for 5 min. 20 μg of protein was loaded and separated by electrophoresis on a 15% (w/v) polyacrylamide gel. The transfer of proteins to nitrocellulose filters and reaction with antibodies were performed as described above. The detection of proteins of total cell lysate was carried out with ECL reagents (Amersham Biosciences).

The antibodies used were as follows: rabbit polyclonal cytochrome *c* antibodies supplied in the ApoAlert cell fractionation kit (1:1,000; BD Biosciences), and rabbit polyclinal VDAC antibodies (1:5,000; Abcam, Cambridge, MA) and mouse monoclonal β-actin antibodies (1:5,000; clone AC-15, SIGMA, St Louis, MO, USA) as primary antibodies, and anti-rabbit IgG alkaline phosphatase conjugate (1:5,000; Bio-Rad Laboratories, CA, USA) as the secondary antibodies for the detection of mitochondrial proteins with an alkaline phosphatase system.

Data Analysis—Statistical analyses were performed using one-way ANOVA coupled with Tukey's pairwise comparisons. A P value of less than 0.05 was considered statistically significant.

RESULTS

The Effects of Heme Synthesis Inhibitors on the Differentiation of Neuro2a—In this study we used Neuro2a cells, because they differentiate on the addition of 20 μM retinoic acid (*15–17*) and detailed information during differentiation after retinoic acid treatment (96 h) has been presented (*17*). As shown in Fig. 1a, morphologic changes such as neurite sprouting and extension after retinoic acid exposure were observed during this period (0–96 h).

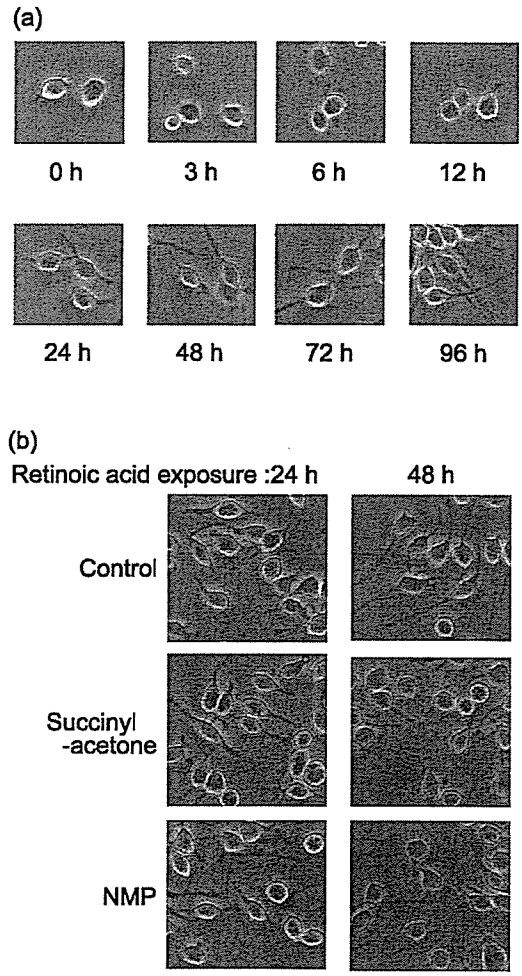

Fig. 1. **a: Retinoic acid–induced differentiation of Neuro2a cells.** The differentiation of Neuro2a cells was induced with 20 μM retinoic acid in Dulbecco's modified Eagle's medium containing 2% (v/v) fetal bovine serum. 0 h means before retinoic acid treatment, that is cells were proliferating, and was considered as a control. Cells at 3 h, 6 h, 12 h, 24 h, 48 h, 72 h and 96 h after the onset of retinoic acid exposure were analyzed to study the differentiation process. **b: The effect of heme biosynthetic inhibitors on retinoic acid–induced differentiation of Neuro2a cells.** Neuro2a cells were either treated with 20 μM retinoic acid alone (control), 20 μM retinoic acid and 1 mM succinyl-acetone (succinyl-acetone), or 20 μM retinoic acid and 10 μM NMP (NMP) for 24 h or 48 h.

As described previously, NGF-induced differentiation of PC12 cells and SHSY5Ycells does not proceed when the precursor cells are exposed to succinyl-acetone or *N*-methylprotoporphyrin IX (NMP), an inhibitor of heme biosynthesis (*11, 12, 22*). To determine whether or not the differentiation of Neuro2a cells was also interfered with heme synthesis inhibitors, the differentiation of Neuro2a cells was compared in the presence and absence of heme biosynthesis inhibitors (Fig. 1b).

As shown in Fig. 1a, neurite sprouting and extension of control cells, which had been treated under normal differentiation conditions (given in materials and methods), were observed within 24 h and further neurite extension was observed thereafter (48, 72, 96 h). In the presence of 1 mM succinyl-acetone or 10 μM NMP, neurite sprouting and extension were observed to 24 h. However, further extension or maintenance of the neurites did not continue to 48 h after the onset of differentiation induction. Under normal growth conditions (without retinoic acid), no difference was observed morphologically between the conditions with and without heme synthesis inhibitors (data not shown).

Expression of mRNAs for Heme Biosynthetic Enzymes during Neuronal Differentiation—To study heme biosynthetic activity during neuronal differentiation, we examined the mRNA levels for eight heme biosynthetic genes (Fig. 2). The mRNA levels of most of the heme biosynthetic enzymes increased during differentiation (Fig. 3). No change was observed in the mRNA level for porphobilinogen deaminase. ALAS, coproporphyrinogen oxidase, and protoporphyrinogen oxidase were more up-regulated than the other enzymes. Increases in the mRNA levels were observed within 48 h, and no further increases were observed thereafter.

Changes in the Heme a *and* b *Contents during Neuronal Differentiation*—To examine the changes in cellular heme contents, non-covalently bound heme (types *a* and *b*) was extracted from cells exposed to retinoic acid for 0–96 h and then quantitatively analyzed by HPLC (Fig. 4). As shown in Fig. 4a and b, in the early phase of differentiation (within 6 h), the heme *a* and *b* contents slightly decreased. A gradual increase in the cellular heme *b* level was observed between 12 and 48 h, and a clear increase was evident after 72 h. In contrast, the heme *a* content did not change significantly during retinoic acid–induced differentiation.

Next we examined the mitochondrial heme content to determine whether or not the change in the cellular heme *b* content was due to the alteration of the amount of mitochondrial heme proteins, such as those of respiratory enzymes (Fig. 4, c and d). Mitochondrial heme *b* also decreased in the early phase of differentiation. However, a low level of heme *b* continued longer than the cellular level (to 24 h) and, unlike the cellular heme *b* level, mitochondrial heme *b* did not reach a higher level than that of 0 h even in the later phase (72, 96 h), although recovery was observed from 48 to 96 h after the onset of differentiation induction. The mitochondrial heme *a* level did not change significantly, although a slight decrease and increase were observed in the early phase and later phase of differentiation, respectively.

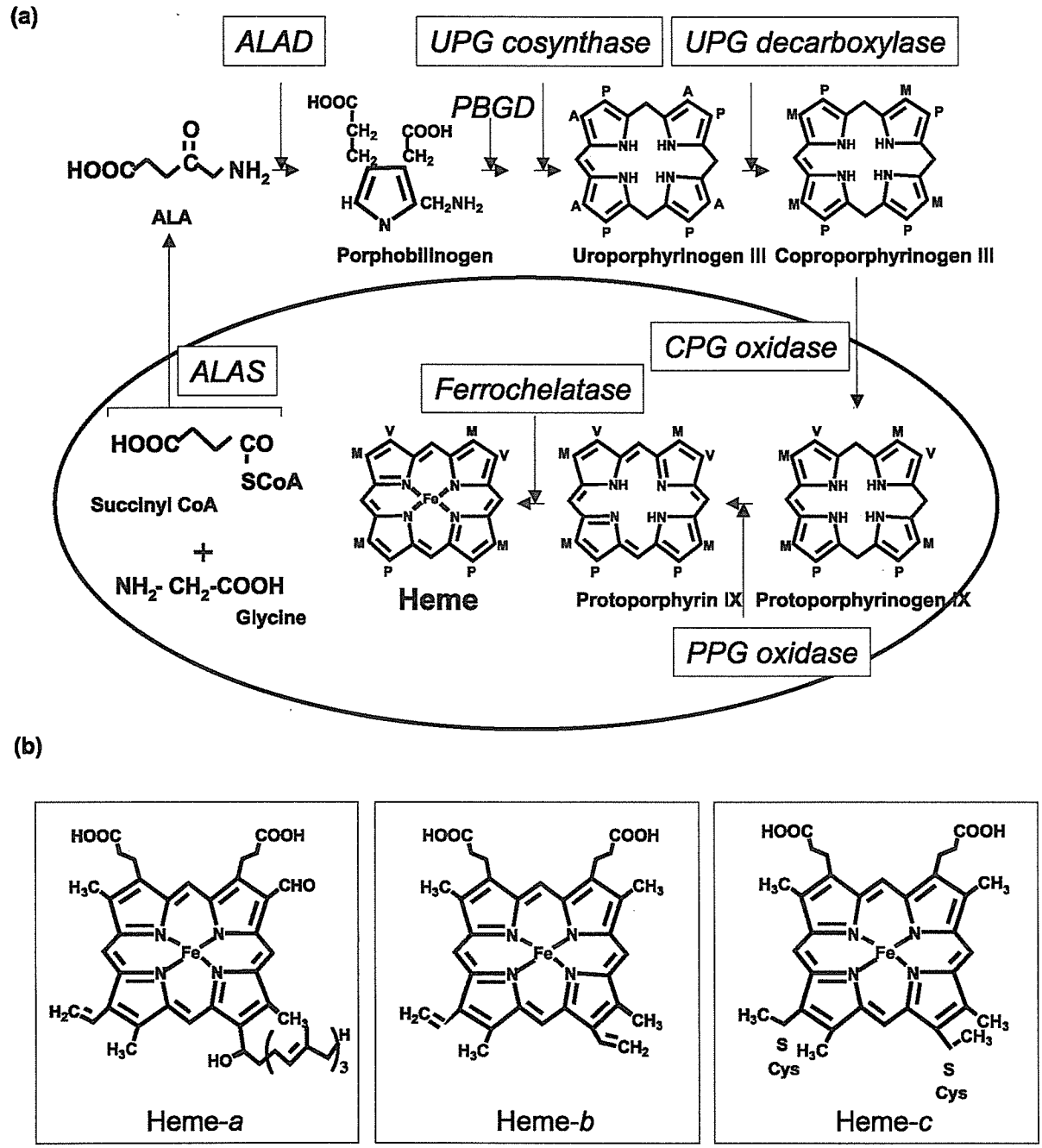

Fig. 2. **a: Heme biosynthetic pathway in mammals.** The enzymes are compartmentalized between the mitochondria and cytosol, with the first enzyme (ALAS) and the last three enzymes located in the mitochondria. ALAS catalyses the conversion of succinyl CoA and glycine to ALA. The last enzyme, ferrochelatase, catalyses the insertion of a ferrous ion into protoporphyrin IX to form heme. ALA, 5-aminolevulinic acid; PBGD, porphobilinogen deaminase; ALAD, 5-aminolevulinic acid dehydratase; UPG, uroporphyrinogen; CPG, coproporphyrinogen; PPG, protoporphyrinogen; A, acetyl; M, methyl; V, vinyl; P, propionyl. **b: The structures of heme *a*, *b*, and *c*.** The structures of the three heme types are shown. Cys in the heme *c* structure are the cystein residues of cytochrome *c* proteins.

Change in Mitochondrial Heme c during Differentiation—In contrast to hemes *a* and *b*, heme *c* cannot be extracted with acetone-HCl because it is covalently attached to the protein. Therefore, heme *c* was detected using the method specific for *c*-type cytochrome involving ECL as described under Materials and methods. Since heme *c* (cytochrome *c* and c_1) is localized in mitochondria and the sensitivity of the heme staining method is too low

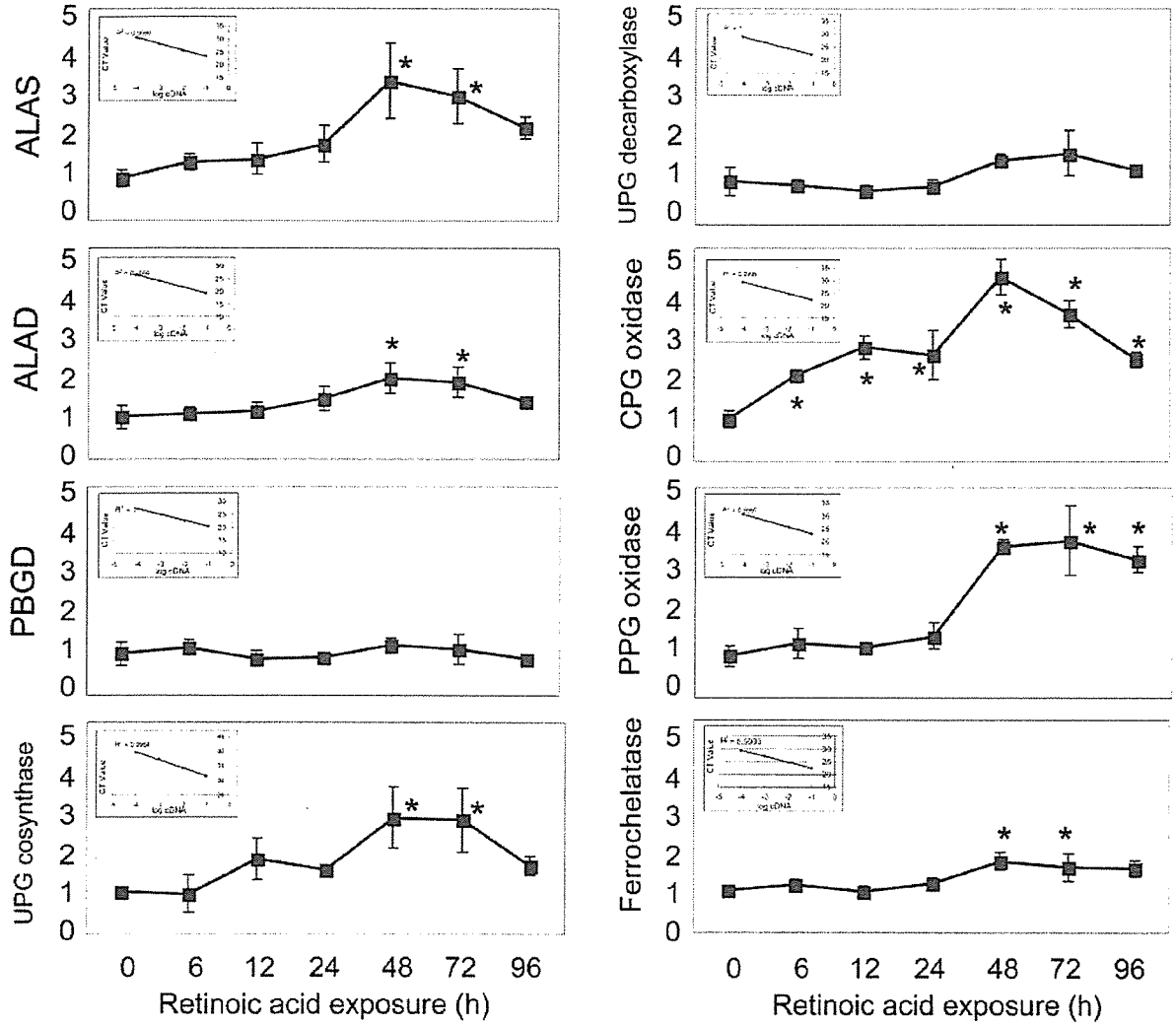

Fig. 3. **mRNA levels of heme biosynthetic enzymes.** Total RNA was extracted from differentiating cells, and cDNA was prepared by reverse transcription. Determination of mRNA levels was performed by real-time PCR. The mRNA levels were normalized as to the levels of β-actin mRNA. The results represent the means ± SD (n = 3). A representative standard curve for each enzyme is shown in the inset. *P < 0.05 *vs.* 0 h, **P < 0.05 *vs.* 6 h (ANOVA followed by Tukey's pairwise comparisons).

to detect cellular heme *c*, we prepared mitochondria from differentiating cells for analysis.

The only heme *c* band observed after ECL staining was one corresponding to a molecular mass of 12 kDa, which corresponds to cytochrome *c* (Fig. 5a, lower panel). This was confirmed by Western blotting with cytochrome *c* specific antibodies (Fig. 5a, upper panel). The level of mitochondrial heme *c* (cytochrome *c*) increased during differentiation, whereas the content of control protein (VDAC) did not change. It is of interest to note that cytochrome *c* rapidly increased during the early phase of differentiation (within 12 h of retinoic acid exposure) in contrast to hemes *a* and *b*. A band corresponding to cytochrome c_1 (27 kDa) was not obsreved. This may be due to the low content of cytochrome c_1 in the mitochondria (*23*).

We next examined the level of cellular cytochrome *c* protein (Fig. 5b). In contrast to the level of mature cytochrome *c* protein in mitochondria, the level of cytochrome *c* polypeptide in the total cell lysate did not increase significantly in the early phase of differentiation (0–12 h), although an obvious increase was observed in the later phase (72–96 h).

DISCUSSION

In the current study, we examined the changes in the heme contents and mRNA levels of heme biosynthetic enzymes to determine the significance of heme synthesis during neuronal differentiation. For these investigations, we used retinoic acid-treated Neuro2a cells as a model of neuronal differentiation.

Neuro2a cells can be induced to differentiate into neuron-like cells with neurites by the addition of retinoic acid (*15–17*). A morphologic change and an increase in acetylcholine-esterase activity, which is a marker for

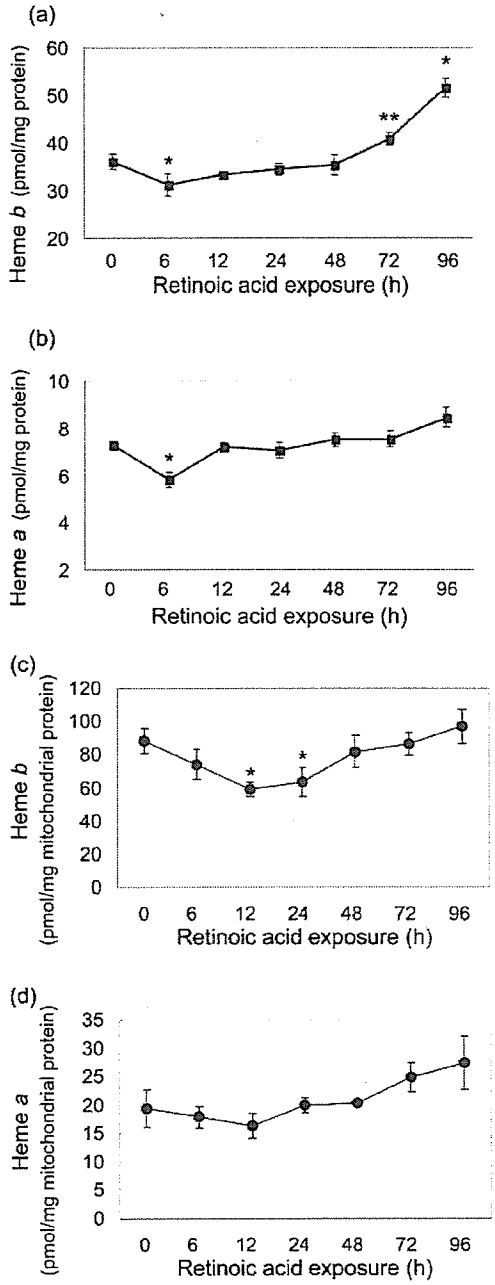

Fig. 4. **Levels of hemes *b* and *a* in differentiating Neuro2a cells.** The heme *b* (a) and heme *a* (b) contents of total cells, and heme *b* (c) and heme *a* (d) contents of mitochondria were determined. The values are normalized as to protein (mg) and the means ± SD (n = 3) are shown. *P < 0.05 *vs.* 0 h, **P < 0.05 *vs.* 6 h (ANOVA followed by Tukey's pairwise comparisons).

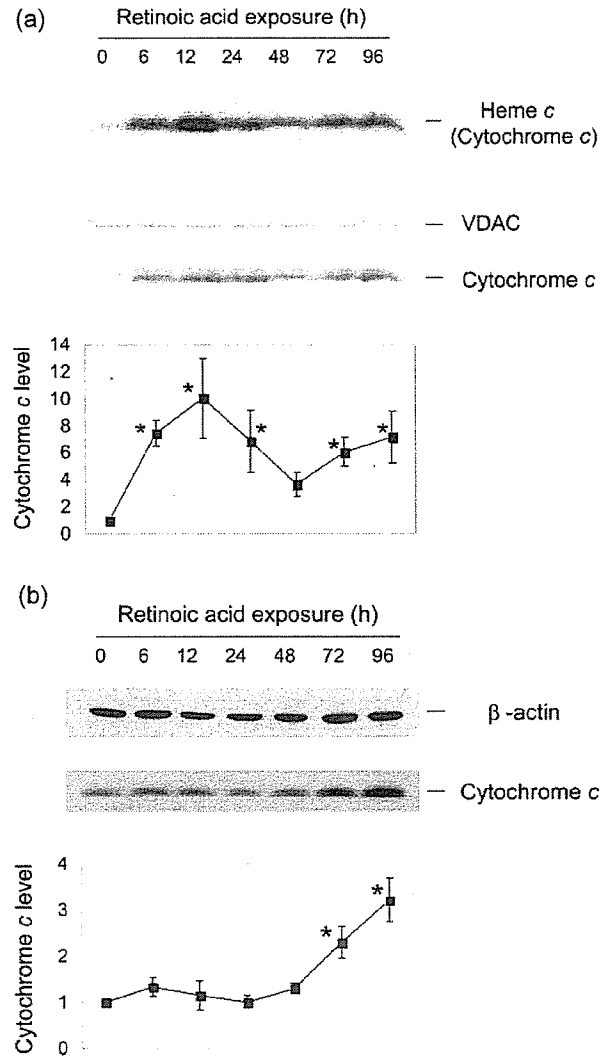

Fig. 5. **Changes in mitochondrial heme *c*, cellular cytochrome *c*, and cytochrome *c* mRNAs in differentiating Neuro2a cells.** (a) Mitochondrial proteins were separated by SDS-PAGE on a 10–20% gradient gel and then transferred to nitrocellulose filter. Heme *c* was detected by means of enhanced chemiluminescence (upper panel). Western blotting was performed with anti-voltage-dependent anion channel (VDAC; control protein) and anti–cytochrome *c* antibodies (middle two panels). Cytochrome *c* levels obtained on densitometric analysis (NIH Image 1.62) are also shown in comparison with the values at 0 h (lower panel). (b) Proteins in total cell lysates were separated by SDS-PAGE on a 15% gel, and cytochrome *c* (lower panel) and β-actin (upper panel) were detected by means of enhanced chemiluminescence using anti–cytochrome *c* and anti β-actin antibodies. The results for the mitochondrial and cellular cytochrome *c* levels represent means ± SD (n = 3). *P < 0.05 *vs.* 0 h.

cholinergic neuron-like differentiation of Neuro2a cells (*24, 25*) were observed (*17*) after retinoic acid treatment (days 0–4). Neurites continued to grow during the period (days 0–4) and the activity of acetylcholine-esterase increased to day 3, but no further activation was observed from day 3 to day 4. We have cultured Neuro2a cells under the same conditions and studied them for 0–96 h after the onset of induction, which corresponds to "days 0–4" (*17*), because the differentiation of Neuro2a cells as cholinergic neuron-like cell occurred from start to 72 h, and neurite extension

and maintenance of neuron-like cells continued to at least 96 h after the onset of induction.

Heme synthesis is known to be regulated during the differentiation of erythroid precursors. In these cells, the first step of the heme biosynthetic pathway, ALAS, is mediated by an erythroid-specific gene (ALAS-2). mRNA expression of ALAS-2 is highly up-regulated during erythroid differentiation to satisfy the cellular demands for heme. Nonerythroid cells, however, do not express ALAS-2. Instead, housekeeping ALAS (ALAS-1) functions as the first enzyme in the heme synthetic pathway. Like ALAS-2, the ALAS-1 level is regulated at the mRNA level: the stability of ALAS-1 mRNA is regulated by the free heme concentration (*26*, *27*), and its transcription is regulated according to the cellular demands for heme (*28*, *29*).

In this study, we found that the expression of ALAS-1 mRNA was up-regulated during neuronal differentiation, whereas the mRNA for ALAS-2 could not be detected. Because the ALAS-1 mRNA level is controlled by the cellular heme concentration (*26*, *27*), the increase in the ALAS-1 mRNA level may be related to enhanced mRNA stability due to the lower level of free heme (heme *b*) that was observed immediately after the induction of differentiation. In addition, the mRNA level for the downstream rate-limiting enzyme coproporphyrinogen oxidase was significantly increased, and a significant increase in protoporphyrinogen oxidase mRNA was also detected. The significance of the increases in the mRNA levels of these downstream enzymes is not clear, because there is little information about the regulation of these enzymes. However, since ALAS and coproporphyrinogen oxidase are rate-limiting enzymes for heme biosynthesis (*30*), it was supposed that activation of the heme synthetic pathway occurs during the differentiation of Neuro2a cells. Because the highest mRNA levels of several heme synthetic enzymes were observed around 48 h after differentiation induction, a high level of heme biosynthesis might be required around this time point.

Heme is an essential prosthetic group for many proteins, such as mitochondrial respiratory enzymes, globin proteins, and some oxidoreductases. Neuronal differentiation consumes a great deal of energy because of the many morphological and functional changes. Therefore, it is not surprising that heme biosynthesis should be enhanced to maintain energy production by the mitochondrial respiratory chain. However compared with the cellular heme *b* level, no significant increase in the mitochondrial heme *b* level was observed. The content of mitochondria per cell does not seem to increase during differentiation, because the only source of heme *a* is complex IV of the mitochondrial respiratory system, and both mitochondrial heme *a* and cellular heme *a* did not increase significantly. Therefore it was supposed that the increase in the cellular heme *b* level in the later phase of differentiation was not due to the triggering of mitochondrial respiration. An elevated heme *b* level may be needed for the production of neuron-specific heme proteins, including neuroglobin and neuronal nitric oxide synthase (*8*, *31*), or essential for expression of the key neuronal gene (*13*).

The most interesting observation in this study was the significant increase in heme *c* during the early phase of differentiation. The cytochrome *c* increase occurred prior to the increases in the mRNA levels of heme biosynthetic enzymes and at the same time as the decrease in heme *b*. In addition, succinyl-acetone, a heme biosynthesis inhibitor, did not interfere with the mitochondrial cytochrome *c* increase in the very early phase of differentiation (3 h after the onset of induction), although the decreases in the heme *a* and *b* levels were accelerated (data not shown). These results suggest that the increased localization of cytochrome *c* proteins in mitochondria was independent of the heme level, at least in the initial phase of differentiation. Cytochrome *c* is encoded in the nucleus, synthesized in the cytoplasm as apo-cytochrome *c* (lacking heme), and then translocated to the mitochondria. During or after mitochondrial import, heme is covalently attached *via* thioether linkages to two cysteine residues in the cytochrome *c* protein (*32*) and mature cytochrome *c* (holocytochrome *c*) is formed. The increased localization of cytochrome *c* proteins in mitochondria found in this study suggested that heme was preferentially consumed for the cytochrome *c* maturation in the early phase of differentiation. We also examined the level of cellular cytochrome *c* protein including apo- and holo-cytochrome *c* during differentiation. It was found that the cellular cytochrome *c* level did not change significantly during the early phase of differentiation, suggesting that the increase in cytochrome *c* is due to changes in post-translational steps, such as mitochondrial transport or heme attachment.

Because hemes *a* and *b* did not increase during this early period, the other components of the mitochondrial respiratory chain are also not expected to increase. Thus, it is unlikely that this increase in cytochrome *c* reflects activation of the respiratory chain. This leaves the question of what is the significance of this drastic increase in cytochrome *c*. Cytochrome *c* has many other roles besides acting as a component of the respiratory chain. For example, it is a scavenger of oxygen free radicals (*33*, *35*). Cytochrome *c* also interacts with the mitochondrial permeability transition pore (*36*, *37*), which forms the site of contact between the inner and outer mitochondrial membranes, and mediates the passage of metabolites between the mitochondria and the cytosol. This pore is known to participate in the release of apoptogenic factors during apoptosis, but its function as a calcium transporter in intracellular signaling has also been suggested (*38*). The physiological role and regulation of the mitochondrial cytochrome *c* increase should be elucidated, and the distribution of apo- and holo-cytochrome *c* in the early phase of nerve cell differentiation is now under investigation.

Neuronal differentiation is important not only for nerve development but also for nerve regeneration. Recently, it was shown that the central nervous system can regenerate due to the ability of precursor cells to differentiate into neurons and thereby compensate for damaged cells (*39*). This regenerating capacity should help protect the central nervous system from damage and stress related to aging. This could explain the reported correlation between the loss of heme and aging in the brain (*22*).

In this study, alterations of heme *a*, *b* and *c* metabolism, and the significance of heme biosynthesis during retinoic acid-induced neuronal differentiation of Neuro2a cells were suggested. This is the first report showing such changes, although other studies have demonstrated the

importance of heme and the heme biosynthetic system in neuronal cells (*11–13, 22, 40*).

This study was supported by Grants-in-Aid for Scientific Research on Priority Areas from the Japanese Ministry of Education, Science, Culture, and Sports (13226015 and 13854011) and The 21st Century COE Program. We also thank Drs. H. Bito and T. Iwatsubo for the helpful discussions and suggestions, and Drs. H. Arai and Y. Takanezawa for providing the Neuro2a cells.

REFERENCES

1. Zhang, L., Hach, A., and Wang, C. (1998) Molecular mechanism governing heme signaling in yeast: a higher-order complex mediates heme regulation of the transcriptional activator HAP1. *Mol. Cell. Biol.* **18**, 3819–3828
2. Gilles-Gonzalez, M.A. and Gonzalez, G. (2005) Heme-based sensors: defining characteristics, recent developments, and regulatory hypotheses. *J. Inorg. Biochem.* **99**, 1–22
3. Maurer, I., Zierz, S., and Moller, H.J. (2000) A selective defect of cytochrome c oxidase is present in brain of Alzheimer disease patients. *Neurobiol. Aging* **21**, 455–462
4. Cottrell, D.A., Blakely, E.L., Johnson, M.A., Ince, P.G., and Turnbull, D.M. (2001) Mitochondrial enzyme-deficient hippocampal neurons and choroidal cells in AD. *Neurology* **57**, 260–264
5. Parker, W.D. Jr., Mahr, N.J., Filley, C.M., Parks, J.K., Hughes, D., Young, D.A. and Cullum, C.M. (1994) Reduced platelet cytochrome c oxidase activity in Alzheimer's disease. *Neurology* **44**, 1086–1090
6. Mutisya, E.M., Bowling, A.C., and Beal, M.F. (1994) Cortical cytochrome oxidase activity is reduced in Alzheimer's disease. *J. Neurochem.* **63**, 2179–2184
7. Howlett, D., Cutler, P., Heales, S., and Camilleri, P. (1997) Hemin and related porphyrins inhibit beta-amyloid aggregation. *FEBS Lett.* **417**, 249–251
8. Laufs, T.L., Wystub, S., Reuss, S., Burmester, T., Saaler-Reinhardt, S., and Hankeln, T. (2004) Neuron-specific expression of neuroglobin in mammals. *Neurosci Lett.* **362**, 83–86
9. Alderton, W.K., Cooper, C.E., and Knowles R.G. (2001) Nitric oxide synthases: structure, function and inhibition. *Biochem. J.* **357**, 593–615
10. Ishii, D.N. and Maniatis, G.M. (1978) Haemin promotes rapid neurite outgrowth in cultured mouse neuroblastoma cells. *Nature* **274**, 372–374
11. Zhu, Y., Hon, T., Ye, W., and Zhang, L. (2002) Heme deficiency interferes with the Ras-mitogen-activated protein kinase signaling pathway and expression of a subset of neuronal genes. *Cell Growth Differ.* **13**, 431–439
12. Zhu, Y., Lee, H.C., and Zhang, L. (2002) An examination of heme action in gene expression: heme and heme deficiency affect the expression of diverse genes in erythroid k562 and neuronal PC12 cells. *DNA Cell Biol.* **21**, 333–346
13. Sengupta, A., Hon, T., and Zhang, L. (2005) Heme deficiency suppresses the expression of key neuronal genes and causes neuronal cell death. *Brain Res. Mol. Brain Res.* **137**, 23–30
14. Moraes, C.T., Diaz, F., and Barrientos, A. (2004) Defects in the biosynthesis of mitochondrial heme c and heme a in yeast and mammals. *Biochim. Biophys. Acta* **1659**, 153–159
15. Tsuji, S., Yamashita, T., Tanaka, M., and Nagai, Y. (1988) Synthetic sialyl compounds as well as natural gangliosides induce neuritogenesis in a mouse neuroblastoma cell line (Neuro2a). *J. Neurochem.* **50**, 414–423
16. Riboni, L., Prinetti, A., Bassi, R., Caminiti, A., and Tettamanti, G. (1995) A mediator role of ceramide in the regulation of neuroblastoma Neuro2a cell differentiation. *J. Biol. Chem.* **270**, 26868–26875
17. Sato, C., Matsuda, T., and Kitajima, K. (2002) Neuronal differentiation-dependent expression of the disialic acid epitope on CD166 and its involvement in neurite formation in Neuro2A cells. *J. Biol. Chem.* **277**, 45299–45305
18. Barros, M.H., Carlson, C.G., Glerum, D.M., and Tzagoloff, A. (2001) Involvement of mitochondrial ferredoxin and Cox15p in hydroxylation of heme O. *FEBS Lett.* **492**, 133–138
19. Wainio, W.W. (1970) *The Mammalian Mitochondrial Respiratory Chain*, Academic Press, New York
20. Towbin, H., Staehelin, T., and Gordon, J. (1979) Electrophoretic transfer of proteins from polyacrylamide gels to nitrocellulose sheets: procedure and some applications. *Proc. Natl. Acad. Sci. USA* **76**, 4350–4354
21. Vargas, C., McEwan, A.G., and Downie, J.A. (1993) Detection of c-type cytochromes using enhanced chemiluminescence. *Anal. Biochem.* **209**, 323–326
22. Atamna, H., Killilea, D.W., Killilea, A.N., and Ames B.N. (2002) Heme deficiency may be a factor in the mitochondrial and neuronal decay of aging. *Proc. Natl. Acad. Sci. USA* **99**, 14807–14812
23. Vanneste, W.H. (1966) Molecular proportion of the fixed cytochrome components of the respiratory chain of Keilin-Hartree particles and beef heart mitochondria. *Biochim. Biophys. Acta* **113**, 175–8
24. Kojima, N., Kurosawa, N., Nishi, T., Hanai, N., and Tsuji, S. (1994) Induction of cholinergic differentiation with neurite sprouting by de novo biosynthesis and expression of GD3 and b-series gangliosides in Neuro2a cells. *J. Biol. Chem.* **269**, 30451–30456
25. Hasegawa, T., Yamaguchi, K., Wada, T., Takeda, A., Itoyama, Y., and Miyagi, T. (2000) Molecular cloning of mouse ganglioside sialidase and its increased expression in Neuro2a cell differentiation. *J. Biol. Chem.* **275**, 8007–8015
26. Hamilton, J.W., Bement, W.J., Sinclair, P.R., Sinclair, J.F., Alcedo, J.A., and Wetterhahn, K.E., (1991) Heme regulates hepatic 5-aminolevulinic acid synthase mRNA expression by decreasing mRNA half-life and not by altering its rate of transcription. *Arch. Biochem. Biophys.* **89**, 387–392
27. Cable, E.E., Miller, T.G., and Isom, H.C. (2000) Regulation of heme metabolism in rat hepatocytes and hepatocyte cell lines: delta-aminolevulinic acid synthase and heme oxygenase are regulated by different heme-dependent mechanisms. *Arch. Biochem. Biophys.* **384**, 280–295
28. Varone, C.L., Giono, L.E., Ochoa, A., Zakin, M.M., and Canepa, E.T. (1999) Transcriptional regulation of 5-aminolevulinic acid synthase by phenobarbital and cAMP-dependent protein kinase. *Arch. Biochem. Biophys.* **372**, 261–270
29. Li, B., Holloszy, J.O., and Semenkovich, C.F. (1999) Respiratory uncoupling induces 5-aminolevulinic acid synthase expression through a nuclear respiratory factor-1-dependent mechanism in HeLa cells. *J. Biol. Chem.* **274**, 17534–17540
30. Woodard, S.I. and Dailey, H.A. (2000) Multiple regulatory steps in erythroid heme biosynthesis. *Arch. Biochem. Biophys.* **384**, 375–378
31. Masters, B.S., McMillan, K., Sheta, E.A., Nishimura, J.S., Roman, L.J., and Martasek, P. (1996) Neuronal nitric oxide synthase, a modular enzyme formed by convergent evolution: structure studies of a cysteine thiolate-liganded heme protein that hydroxylates L-arginine to produce NO as a cellular signal. *FASEB J.* **10**, 552–558
32. Stevens, J.M., Daltrop, O., Allen, J.W., and Ferguson, S.J. (2004) C-type cytochrome formation: chemical and biological enigmas. *Acc Chem. Res.* **37**, 999–1007
33. Zhao, Y., and Xu, J.X. (2004) The operation of the alternative electron-leak pathways mediated by cytochrome c in mitochondria. *Biochem. Biophys. Res. Commun.* **317**, 980–987
34. Zhao, Y., Wang, Z.B., and Xu, J.X. (2003) Effect of cytochrome c on the generation and elimination of O_2*- and H_2O_2 in mitochondria. *J. Biol. Chem.* **278**, 2356–2560

35. Tsatmali, M., Walcott, E.C., and Crossin, K.L. (2005) Newborn neurons acquire high levels of reactive oxygen species and increased mitochondrial proteins upon differentiation from progenitors. *Brain Res.* **1040**, 137–50
36. Wieckowski, M.R., Vyssokikh, M., Dymkowska, D., Antonsson, B., Brdiczka, D., and Wojtczak, L. (2001) Oligomeric C-terminal truncated Bax preferentially releases cytochrome c but not adenylate kinase from mitochondria, outer membrane vesicles and proteoliposomes. *FEBS Lett.* **505**, 453–459
37. Vyssokikh, M., Zorova, L., Zorov, D., Heimlich, G., Jurgensmeier, J., Schreiner, D., and Brdiczka, D. (2004) The intra-mitochondrial cytochrome *c* distribution varies correlated to the formation of a complex between VDAC and the adenine nucleotide translocase: this affects Bax-dependent cytochrome c release. *Biochim. Biophys. Acta* **1644**, 27–36
38. Vyssokikh, M.Y. and Brdiczka, D. (2003) The function of complexes between the outer mitochondrial membrane pore (VDAC) and the adenine nucleotide translocase in regulation of energy metabolism and apoptosis. *Acta Biochim. Pol.* **50**, 389–404
39. Nakatomi, H., Kuriu, T., Okabe, S., Yamamoto, S., Hatano, O., Kawahara, N., Tamura, A., Kirino, T., and Nakafuku, M. (2002) Regeneration of hippocampal pyramidal neurons after ischemic brain injury by recruitment of endogenous neural progenitors. *Cell* **110**, 429–441
40. Atamna, H. and Frey, W.H. 2nd (2004) A role for heme in Alzheimer's disease: heme binds amyloid beta and has altered metabolism. *Proc. Natl. Acad. Sci. USA* **101**, 11153–11158

THE JOURNAL OF BIOLOGICAL CHEMISTRY VOL. 281, NO. 3, pp. 1714–1724, January 20, 2006

Identification and Characterization of Amino Acid Residues Essential for the Active Site of UDP-*N*-acetylenolpyruvylglucosamine Reductase (MurB) from *Staphylococcus aureus*[*]

Received for publication, August 23, 2005, and in revised form, September 28, 2005 Published, JBC Papers in Press, October 19, 2005, DOI 10.1074/jbc.M509277200

Satoshi Nishida[‡1], Kenji Kurokawa[‡2], Miki Matsuo[‡], Kimitoshi Sakamoto[§], Kohji Ueno[¶], Kiyoshi Kita[§], and Kazuhisa Sekimizu[‡]

From the [‡]Laboratory of Developmental Biochemistry, Graduate School of Pharmaceutical Sciences, the [§]Department of Biomedical Chemistry, Graduate School of Medicine, University of Tokyo, Tokyo 113-0033, Japan and the [¶]Laboratory of Microbiology, Research Institute of Pharmaceutical Sciences, Musashino University, Tokyo 202-8585, Japan

The enzymes essential for bacterial peptidoglycan biosynthesis are attractive targets for antimicrobial drug development. One of these is MurB, which contains FAD as a cofactor and catalyzes the NADPH-dependent reduction of UDP-*N*-acetylenolpyruvylglucosamine (UDP-GlcNAcEP) to UDP-*N*-acetylmuramic acid. This study examined the roles of the conserved amino acid residues of *Staphylococcus aureus* MurB, which are located near the active site in x-ray crystal structures. Seven of 11 site-directed mutated *murB* genes lost the ability to complement a temperature-sensitive *S. aureus murB* mutant. Biochemical characterization of the seven mutated MurB proteins revealed that they cannot carry out the reduction of UDP-GlcNAcEP, although they can all catalyze the intramolecular reduction of FAD via NADPH. Spectrometric analyses of the oxidized form of the mutated proteins in the presence and absence of $NADP^+$ or UDP-GlcNAcEP revealed that these essential amino acid residues play four distinct roles in substrate interactions: Arg^{213} is essential for maintenance of the electronic state of FAD; Arg^{176} is required for interaction with UDP-GlcNAcEP; His^{259} is required for interaction with both UDP-GlcNAcEP and $NADP^+$; and Asn^{71}, Tyr^{175}, Ser^{226}, and Glu^{296} are not apparently required for interaction with either ligand. The results presented here identify for the first time the amino acid residues of MurB that are required for the interaction with UDP-GlcNAcEP and $NADP^+$.

The expansion of infectious diseases caused by multidrug-resistant *Staphylococcus aureus* and other pathogenic bacteria has become an increasing global problem. Thus, the development of antibacterial drugs that have novel mechanisms of action or targets is needed. Peptidoglycan is a component of the bacterial cell wall and prevents cell lysis caused by high intracellular pressure. Because the enzymes responsible for peptidoglycan biosynthesis are ubiquitous in bacteria but are not found in humans, they are expected to be good targets for antibacterial drug development.

Peptidoglycan consists of a saccharide backbone that is formed by alternating *N*-acetylglucosamine and *N*-acetylmuramic acid residues with tetra- or pentapeptides that branch from *N*-acetylmuramic acid (1–3). In *S. aureus*, L-lysine of one of the tetrapeptides is cross-linked to D-alanine of the other by a pentaglycine chain. The initial step of peptidoglycan biosynthesis is the conversion of UDP-*N*-acetylglucosamine and phosphoenolpyruvate to UDP-*N*-acetylenolpyruvylglucosamine (UDP-GlcNAcEP)[3] by MurA. Subsequently, UDP-GlcNAcEP is reduced to UDP-*N*-acetylmuramic acid by MurB. Next, five amino acid residues (L-Ala, D-Glu, L-Lys, and D-Ala-D-Ala) are sequentially added onto the D-lactyl group of UDP-*N*-acetylmuramic acid by MurC, MurD, MurE, and MurF enzymes in a ribosome-independent manner.

Because MurB is one of the essential enzymes for peptidoglycan biosynthesis (4–6), chemical compounds that block MurB function are candidate antimicrobial agents (7, 8). Several inhibitors have been designed based on the crystal structure of the UDP-GlcNAcEP-MurB complex (9, 10). However, it has not yet been determined whether MurB-targeting drugs are clinically effective.

MurB is a flavoprotein that belongs to the FAD-binding protein superfamily, which shares a characteristic FAD binding fold (11). The MurB family is divided into at least two groups by amino acid sequence alignment: type I, which includes *Escherichia coli* MurB; and type II, which includes *S. aureus* MurB. This latter type lacks both a loop structure containing Tyr^{190} and a single split $\beta\alpha\beta\beta$ fold, which are found in the substrate binding domain of type I *E. coli* MurB (12). X-ray structural analyses indicated that the *E. coli* type I and *S. aureus* type II MurB proteins have similar overall folds, although there are differences between the substrate binding regions due to amino acid deletions (12, 13).

The enzyme reaction catalyzed by MurB is performed by Ping Pong Bi Bi mechanism, alternatively Ping Pong Tetra Uni in the Cleland system of nomenclature; the first step is the reduction of FAD, which consumes one equivalent of NADPH, and the second is an electron transfer from $FADH_2$ to UDP-GlcNAcEP (14). In this mechanism, both NADPH and UDP-GlcNAcEP bind to the same subdomain (15, 16) (Fig. 1). Ser^{229} in *E. coli* MurB, which corresponds to Ser^{226} in *S. aureus* MurB, is a catalytic residue and participates in the proton transfer to an enol intermediate that is formed during the second reduction step (17, 18).

Experimental evidence for essential amino acid residues and their

[*] This work was supported in part by Grants-in-Aid for Scientific Research from the Japan Society for the Promotion of Science and by the Industrial Technology Research Grant Program in '04 from the New Energy and Industrial Technology Development Organization of Japan. The costs of publication of this article were defrayed in part by the payment of page charges. This article must therefore be hereby marked "*advertisement*" in accordance with 18 U.S.C. Section 1734 solely to indicate this fact.

[1] Present address: Laboratory of Microbiology, Research Institute of Pharmaceutical Sciences, Musashino University, Tokyo 202-8585, Japan.

[2] To whom correspondence should be addressed: Laboratory of Developmental Biochemistry, Graduate School of Pharmaceutical Sciences, The University of Tokyo, 7-3-1, Hongo, Bunkyo-ku, Tokyo 113-0033, Japan. Tel.: 81-3-5841-4821; Fax: 81-3-5684-2973; E-mail: kurokawa@mol.f.u-tokyo.ac.jp.

[3] The abbreviations used are: UDP-GlcNAcEP, UDP-*N*-acetylenolpyruvylglucosamine; HPLC, high pressure liquid chromatography.

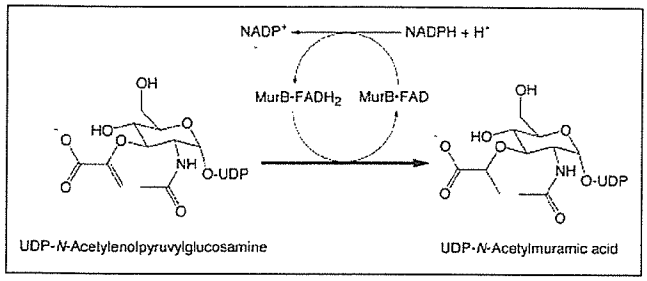

FIGURE 1. **Reaction catalyzed by MurB.**

roles in the enzyme activity as well as protein structural information is critical for developing enzyme-specific antibacterial drugs. Amino acid residues located in or close to substrate binding sites, which are revealed by x-ray or NMR structural analysis, are not always essential for the enzyme activity. In this study, we examined whether the amino acid residues of *S. aureus* MurB, which are well conserved among various bacterial MurB proteins and are located close to the catalytic site, are essential for catalytic activity. Site-specifically mutated *S. aureus murB* genes were constructed and tested for the ability to complement a temperature-sensitive *murB* mutant of *S. aureus* (6). Seven residues, including Asn^{71}, Tyr^{175}, Arg^{176}, Arg^{213}, Ser^{226}, His^{259}, and Glu^{296}, were found to be essential for activity. Purification and biochemical analyses of these mutated proteins revealed that each could carry out the NADPH-dependent reduction of FAD but that they could not complete the subsequent reduction of UDP-GlcNAcEP. Furthermore, the roles of each essential residue in the interaction of MurB with $NADP^+$ and UDP-GlcNAcEP were examined by differential spectral analyses of intramolecular FAD. This allowed classification of the essential residues into four functional groups.

EXPERIMENTAL PROCEDURES

Reagents—All reagents were of analytical grade. Glucose oxidase, catalase, $NADP^+$, NADPH, and protein molecular weight markers were purchased from Sigma. DEAE-Sepharose CL-6B and monoQ HR5/5 columns were from Amersham Biosciences. UDP-GlcNAcEP was synthesized *in vitro* from UDP-*N*-acetylglucosamine and phosphoenolpyruvate using purified *S. aureus* MurA1 and isolated by high pressure liquid chromatography (HPLC). The UDP-GlcNAcEP was calculated according to the UV absorbance at 262 nm as described previously (6).

Strains and Growth Conditions—E. coli strain JM109 (*recA1, endA1, gyrA96, thi, hsdR17, supE44, relA1,* Δ(*lac-proAB*)/F′ [*traD36, proAB*$^+$, *lacI*^{q}, *lacZ*ΔM15]) was used as a host for plasmid construction, and BL21 (DE3)/pLysS (F$^-$, *ompT, hsdS, gal* [λ *cI857, ind1, Sam7, nin5, lacUV5-T7gene1*], *dcm*[DE3]) (Novagen) was used for the overproduction of MurB proteins. The *S. aureus* temperature-sensitive *murB* mutant was derived from RN4220 (6). *E. coli* and *S. aureus* cells were grown in LB medium containing 1% (w/v) bactotryptone, 0.5% (w/v) yeast extract, and 1% (w/v) NaCl with 50 μg/ml ampicillin or 12.5 μg/ml chrolamphenicol as needed.

General Techniques—Ligation was performed using a DNA ligation kit (version 2; Takara). KOD plus DNA polymerase (Toyobo) or *Pfu* DNA polymerase (Stratagene) was used for PCRs. DNA sequencing was performed using a PRISM 3100 DNA sequencer and PRISM BigDye terminator cycle sequencing kit version 3.0 (PerkinElmer Life Sciences). Protein determination was performed by the Bradford method using the Bio-Rad protein assay and bovine serum albumin (Sigma) as a standard.

Site-directed Mutagenesis—Site-directed mutagenesis of the *S. aureus murB* gene was performed by the overlap extension method (19). Shown in Table 1 are the oligonucleotide sequences used, which were

TABLE 1
Primers used for site-directed mutagenesis of MurB

Mutation	Primer DNA sequence[a]
G67A	5′-GTTACATATTTAGCAAATGGCTCAAAT-3′
	5′-ATTTGAGCCATTTGCTAAATATGTAAC-3′
G69A	5′-ATTTAGGAAATGCCTCAAATATTATT-3′
	5′-AATAATATTTGAGGCATTTCCTAAAT-3′
S70A	5′-TTAGGAAATGGCGCAAATATTATT-3′
	5′-AATAATATTTGCGCCATTTCCTAA-3′
N71A	5′-AGGAAATGGCTCAGCTATTATTATCCGTG-3′
	5′-CACGGATAATAATAGCTGAGCCATTTCCT-3′
Y175F	5′-TAGAGTTAGATTTTCGTAATAGCATT-3′
	5′-AATGCTATTACGAAAATCTAACTCTA-3′
R176A	5′-AGAGTTAGATTATGCTAATAGCATTATTC-3′
	5′-GAATAATGCTATTAGCATAATCTAACTCT-3′
R213A	5′-TTAACAGAACGTGCAGAATCTAAACA-3′
	5′-TGTTTAGATTCTGCACGTTCTGTTAA-3′
S226A	5′-CCTTCATGTGGTGCTGTATTCCAAAG-3′
	5′-CTTTGGAATACAGCACCACATGAAGG-3′
R230A	5′-AGTGTATTCCAAGCACCGCCTGGTC-3′
	5′-GACCAGGCGGTGCTTGGAATACACT-3′
H259A	5′-GAAGTTTCAACCAAAGCCGCTGGTTTTATGGT-3′
	5′-ACCATAAAACCAGCGGCTTTGGTTGAAACTTC-3′
E296A	5′-GAATTAAATCGTGCAGTTCGCATT-3′
	5′-AATGCGAACTGCACGATTTAATTC-3′

[a] The underlined bases indicate the nucleotide positions that were changed.

complementary internal primers that had 20-bp overlaps with the mutation site. The first round PCRs (15 cycles) were carried out using the upper primer of each construction in Table 1 paired with the murB3 primer, 5′-CCG**GAATTC**ATAATGGCGACAGCGTGTTT-3′, corresponding to the 3′-end of the *murB* gene containing the EcoRI site (in boldface type) and the lower primer paired with the murB5 primer, 5′-TCAACTAATGATGATATTGCTTTGC-3′, corresponding to the upstream sequence of the MurB open reading frame. Each group of two primary PCR products was purified, mixed, and used for the second round of PCR (15 cycles) using the murB5 and murB3 primers, and products were digested with EcoRI and cloned into the pND50 shuttle vector at the EcoRI and SmaI sites. Site-specific mutations on cloned fragments were confirmed by DNA sequencing. The resulting plasmids were designated pNDmurBG67A, pNDmurBG69A, pNDmurBS70A, pNDmurBN71A, pNDmurBY175F, pNDmurBR176A, pNDmurBR213A, pNDmurBS226A, pNDmurBR230A, pNDmurBH259A, and pNDmurBE-296A, respectively.

Complementation Assay—Complementation assays were performed as described previously (6). The *S. aureus murB* temperature-sensitive mutant TS2901 was transformed with 100 ng of plasmids described above, pNDmurBs, and its vector pND50 by electroporation in a 0.2-cm cuvette (Gene Pulser II; Bio-Rad). Transformants were grown on NaCl-free LB agar plates containing 12.5 μg/ml chloramphenicol at 30 or 43 °C. The numbers of transformants were counted after 24 h.

Plasmids for Overexpression of MurB—To construct plasmid series of pETSXmurB for overexpression of *S. aureus* MurB in *E. coli*, the MurB open reading frame was amplified with PCR using the primers for murB3 described above and a primer for murB5N, 5′-GAAAGGATG-TACT**CCATGG**TGATAAATAAA-3′, that incorporated the NcoI site (in boldface type) with the initiation codon and using pSmurB, a plasmid harboring the wild-type *S. aureus murB* gene (6), as a template. The product was digested with NcoI and EcoRI and then ligated into the NcoI and EcoRI sites of pET21d (Novagen), resulting in the plasmid pETmurB. The HindIII site in its multicloning site was removed by digestion with SalI and XhoI and self-ligated. This resulting plasmid was designated pETSXmurB. With regard to the seven mutant *murB* genes that eliminated the ability to complement the temperature-sensitive *S. aureus murB* mutant *in vivo*, each DNA fragment harboring the mutation site was cut off by digestion with HindIII and EcoRI from the respective pND50-based plasmid and exchanged with the correspond-

ing region of pETSXmurB at the HindIII and EcoRI sites. The resulting plasmids were designated pETSXmurBN71A, pETSXmurBY175F, pETSXmurBR176A, pETSXmurBR213A, pETSXmurBS226A, pETSXmurBH259A, and pETSXmurBE296A, respectively.

Purification of S. aureus MurB—BL21 (DE3)/pLysS (Novagen) were transformed with plasmids of the pETSXmurB series. Each strain was grown in 1 liter of LB medium at 37 °C until the A_{600} reached 0.5, after which the culture was adjusted to 0.5 mM isopropyl 1-thio-β-D-galactopyranoside. After a 2-h induction, cells were harvested by centrifugation, washed once with 30 ml of 0.9% NaCl, and frozen in liquid N_2. The frozen cell paste (~3 g) was resuspended and lysed in 6 ml of lysis buffer (50 mM Hepes-KOH, pH 7.6, 1 mM dithiothreitol, 1 mM EDTA, 20% (v/v) glycerol, 0.25 M KCl, 0.3 mg/ml lysozyme (Sigma), and 20 mM spermidine (Sigma)) on ice for 20 min. Samples were again frozen and thawed and then sonicated four times for 30 s using a Branson Sonifier 450. The resulting homogenate was centrifuged at 145,000 × *g* for 30 min at 4 °C, and cleared lysates (Fraction I) were adjusted to 0.3 g/ml ammonium sulfate and stirred for 20 min at 4 °C. After centrifugation at 40,000 × *g* for 20 min, ammonium sulfate was added again to the supernatant to a final concentration of 0.5 g/ml. The precipitate was collected, and the deep yellow pellet was dissolved in buffer C′ (50 mM Hepes-KOH, pH 7.6, 1 mM dithiothreitol, 1 mM EDTA, and 20% (v/v) glycerol) and dialyzed against the same buffer (Fraction II). Fraction II was loaded at a flow rate of 1 ml/min onto a DEAE-Sepharose CL6-B column (1.5 × 10 cm) preequilibrated with buffer C′ and then eluted with a linear gradient from 0 to 0.8 M NaCl in buffer C′. Active wild-type MurB was identified in the 0.2 M NaCl eluate. Pooled MurB (Fraction III) was dialyzed against buffer C′, loaded onto a monoQ HR5/5 column at a flow rate of 0.25 ml/min, and eluted with a linear gradient from 0 to 0.5 M NaCl in buffer C′. Active wild-type MurB again eluted at 0.2 M NaCl and was pooled (Fraction IV). The various mutated forms of MurB were prepared in a similar way, and MurB was followed using the absorbance of FAD at 460 nm. The purity of each Fraction IV exceeded 80% on SDS-PAGE. The protein concentration was determined by the Bradford method using bovine serum albumin as a standard. Proteins were stored at −80 °C.

Enzymatic Assays—A typical aerobic MurB assay was performed as described previously (20) in a reaction mixture (0.1 ml) of 50 mM Tris-HCl (pH 8.0), 20 mM KCl, 0.5 mM dithiothreitol, 0.1 mM UDP-GlcNAcEP, and 0.15 mM NADPH in an open cuvette. Anaerobic reactions were performed as described previously (14) with some modifications. Reactions (0.4 ml) contained 50 mM Tris-HCl (pH 8.0), 20 mM KCl, 0.5 mM dithiothreitol, 0.1 mM UDP-GlcNAcEP, 0.15 mM NADPH, 10 mM D-glucose, 20 units/ml glucose oxidase, and 26 units/ml catalase. The reaction mixtures were added to semimicrocuvettes with Teflon caps (GL Sciences) and flushed with nitrogen gas. After maintaining the mixture at room temperature for 5 min, reactions were started by adding enzyme followed by both flushing with nitrogen gas and capping under a nitrogen atmosphere. Under these conditions, oxygen was scavenged immediately (21).

In each assay, the initial velocity of NADPH oxidation at room temperature was determined by monitoring the decrease in absorbance at 340 nm every 30 or 60 s for 5 min using a UV-160A or a UV-2200 spectrophotometer (Shimadzu) and with 3–30 pmol of MurB. To determine specific activities, an extinction coefficient of 6220 M^{-1} cm^{-1} at 340 nm was used for NADPH. It was confirmed that the absorbance was linear up to 0.27 mM. K_m values for NADPH and UDP-GlcNAcEP were determined as described previously (22).

Determination of FAD Content of MurB—Determination of the FAD content was performed as described previously (23). FAD was released from MurB (Fraction IV; 3 μg) by boiling for 5 min followed by the addition of 70% ethanol. After centrifugation at 10,000 × *g* at room temperature for 5 min to remove denatured proteins, flavin was recovered in the supernatant. The flavin was analyzed by HPLC using a TOSOH analytical C-18 column (TSK-gel ODS-80Ts QA; 4.6 × 250 mm) at a flow rate of 1 ml/min with a solvent of 35% (v/v) methanol, 100 mM formic acid, 100 mM ammonium formate (pH 3.5) using a Hitachi L-7480 fluorescence detector (excitation, 470 nm; emission, 530 nm) and with FAD (Yamasa) as a standard.

Determination of K_d Values of MurB for UDP-GlcNAcEP or $NADP^+$—Determinations of K_d values of wild-type and mutated MurB for either UDP-GlcNAcEP or $NADP^+$ were carried out using difference spectrum analyses as described previously (22). Absorption spectra were recorded with a Shimadzu UV-2200 spectrophotometer at a scan rate of 50 nm/min. MurB at a final concentration of 15–20 nM was assayed in buffer C′ at room temperature. Difference spectra, which can improve both the sensitivity and selectivity to detect the spectral perturbation elicited by ligand binding, were computed from the spectra in the presence and absence of ligand and were corrected for dilution. The absorbance changes at 510 nm as a function of ligand concentration were fitted to the following theoretical equation for a 1:1 binding stoichiometry by nonlinear regression using the Kaleida Graph program (Synergy Software Ltd.), where A represents the measured absorption, A_0 is the starting absorbance, ΔA is the total measured change in absorbance, $[E_0]$ is the enzyme concentration, K_d is the ligand dissociation constant, and $[S_0]$ is the concentration of ligand added to the enzyme.

$$A = A_0 + (\Delta A/E_0)((K_d + [E_0] + [S_0]) - ((K_d + [E_0] + [S_0])^2 - 4[E_0][S_0])^{1/2})/2 \quad \text{(Eq. 1)}$$

Molecular Modeling of Active Site Residues—The *S. aureus* MurB·UDP-GlcNAcEP complex was drawn using Swiss-PdbViewer 3.7, which automatically fitted UDP-GlcNAcEP from the *E. coli* MurB·UDP-GlcNAcEP complex (13) (Protein Data Bank code 2mbr) into the *S. aureus* MurB structure (12) (Protein Data Bank code 1hsk) using a three-dimensional match procedure. The graphic was rendered using POV-Ray 3.6.

RESULTS AND DISCUSSION

Selection of Amino Acid Residues of MurB for Mutational Analyses—Fig. 2 shows the amino acid sequences for several regions of MurB from a number of bacteria, with *boxes* enclosing highly conserved residues. X-ray crystal structure analyses of the *E. coli* MurB·UDP-GlcNAcEP complex and *S. aureus* MurB revealed that most of these conserved residues are located close to the cofactor FAD or substrate UDP-GlcNAcEP binding sites (12, 13). In this study, we selected 11 amino acid residues (Fig. 2) that are highly conserved among both type I and II enzymes and are located near the active sites as residues that may be essential for enzyme activity. We examined this by constructing mutants in which the targeted amino acid was replaced with alanine or, in the case of tyrosine residues, with phenylalanine. Gly^{67}, Gly^{69}, Ser^{70}, Asn^{71}, and Arg^{213} are located close to the FAD biding site, whereas Tyr^{175}, Arg^{176}, Ser^{226}, Arg^{230}, His^{259}, and Glu^{296} are located close to the UDP-GlcNAcEP binding site. Both Asn^{71} and Arg^{213} are near the enolpyruvyl group of UDP-GlcNAcEP. Ser^{226} corresponds to Ser^{229} of *E. coli* MurB, which was reported previously as a catalytic residue whose hydroxyl group is thought to transfer a proton for the reduction of UDP-GlcNAcEP (18).

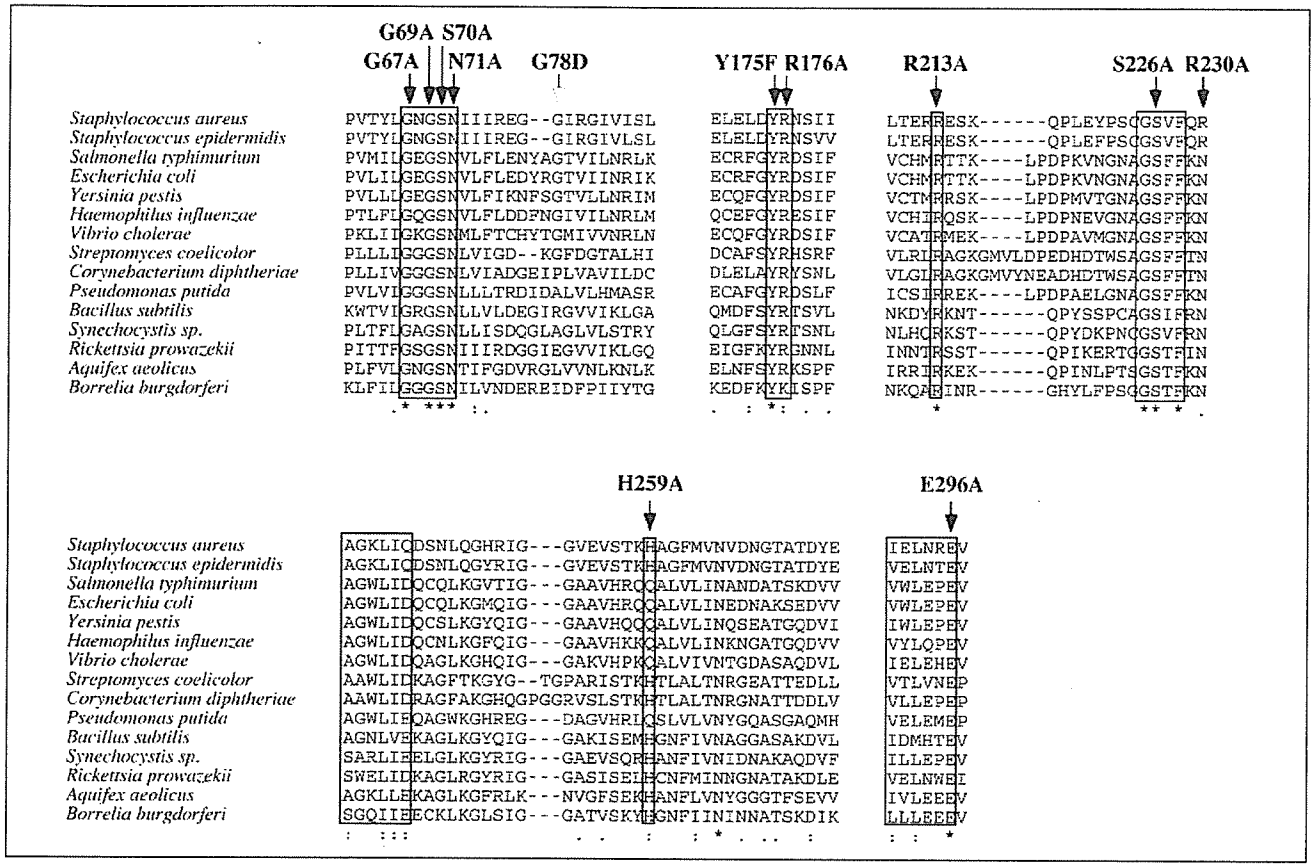

FIGURE 2. **Multiple sequence alignment of *murB* orthologues and mutations.** Alignment of *murB* orthologue sequences was performed using ClustalW. Gaps (-) were introduced to optimize the alignment. *Asterisks*, *colons*, and *periods above* the alignment indicate fully, strongly, and weakly conserved residues, respectively. The *white* and *black arrows* indicate the temperature-sensitive mutation and site-directed mutations in *S. aureus* MurB protein, respectively.

TABLE 2

Activity of mutated forms of MurB *in vivo*

The temperature-sensitive mutant TS2901 of *S. aureus murB* was transformed by electroporation with 100 ng of pND50 vector or pND50-derived plasmid harboring the wild-type or mutated *murB* gene. The numbers of transformants were counted after 24 h at 30 or 43 °C.

murB allele	*E. coli* residue[a]	Efficiency of transformation		43 °C/30 °C ratio
		30 °C	43 °C	
		× 10^4/μg DNA		
G67A	Gly^{47}	3.4	3.8	1.1
G69A	Gly^{49}	4.1	1.9	0.94
S70A	Ser^{50}	0.96	0.95	1.0
N71A	Asn^{51}	4.8	<0.001	<0.0002
Y175F	Tyr^{158}	2.0	0.018	0.009
R176A	Arg^{159}	3.8	0.001	0.0002
S226A	Ser^{229}	3.9	<0.001	<0.0002
R213A	Arg^{214}	3.0	<0.001	<0.0003
R230A	Asn^{233}	4.0	3.9	0.97
H259A	Gln^{288}	4.9	<0.001	<0.0002
E296A	Glu^{325}	0.65	<0.001	<0.001
Wild-type		3.9	5.2	1.3
- (vector)		4.8	<0.001	<0.0002

[a] The corresponding residues for the *E. coli* enzyme are shown.

In Vivo Complementation Test of the Mutated murB Genes with a Temperature-sensitive murB Mutant—We next examined the abilities of the mutated *murB* genes to complement the temperature-sensitive *S. aureus murB* strain TS2901. The TS2901 strain was electroporated with plasmids harboring the *murB* genes, and the transformants were counted (6). Wild-type *murB* gene formed a similar number of transformants at 30 and 43 °C, whereas the empty vector plasmid could not form transformants at 43 °C (Table 2). The number of transformants at 43 °C was less than 1% of that at 30 °C for the N71A, Y175F, R176A, R213A, S226A, H259A, and E296A mutated *murB* genes. On the other hand, similar numbers of transformants were formed at 30 and 43 °C by the G67A, G69A, S70A, and R230A mutants. Thus, it appears that the N71A, Y175F, R176A, R213A, S226A, H259A, and E296A mutants lose MurB activity, whereas G67A, G69A, S70A, and R230A retain the activity.

Gly^{67} and Gly^{69} comprise a Gly-*X*-Gly motif, which is a conserved sequence in the FAD-binding domain of FAD-binding proteins. X-ray structural analysis of *S. aureus* MurB indicates that Gly^{67} and Gly^{69}

TABLE 3
Purification of *S. aureus* MurB protein

Fraction	Purification step	Total protein	Specific activity[a]	Total activity[a]	Yield	Purification
		mg	*units/mg*	*units*	*%*	*-fold*
I	Cell lysate	220	0.46	101	100	1
II	$(NH_4)_2SO_4$ precipitate	44	1.2	51	50	2.6
III	DEAE-Sepharose	15	2.1	32	32	4.6
IV	MonoQ	3.9[b]	4.6	18[b]	18[b]	10

[a] 1 unit = 1 μmol of NADPH oxidized/min.
[b] A quarter of fraction III was applied to a monoQ column.

interact with the α-phosphoryl moiety of FAD by the main-chain nitrogen, and the following residue, Ser^{70}, interacts with the β-phosphoryl moiety of FAD via both its main-chain nitrogen and its side-chain hydroxyl group (12, 13). The fact that both G67A and G69A can complement the temperature-sensitive mutant suggests that the glycine residues of the GXG motif can be replaced with an alanine residue. This result is consistent with the finding that several FAD binding proteins have alanine at glycine positions in the GXG motif (24) and that the main-chain nitrogen of the glycine residues is responsible for the interaction with FAD (12, 13).

Purification of Mutated MurB Proteins—To determine the roles of the essential residues of the *S. aureus* MurB protein, each mutated MurB that was inactive for *in vivo* complementation was expressed in *E. coli* and purified to homogeneity. To follow the purification of wild-type MurB, we measured the specific activity for UDP-GlcNAcEP reductase under aerobic conditions (Table 3). On the last step of column chromatography (monoQ), the MurB proteins eluted with peaks of both A_{460} and A_{280}. The final fraction (Fraction IV) of each mutated MurB protein contained a single 34-kDa band on SDS-polyacrylamide gel electrophoresis (Fig. 3), which is consistent with the molecular mass of *S. aureus* MurB. The purity of all of the isolated MurB proteins was estimated to be greater than 80%.

UDP-GlcNAcEP Reductase Activity of Wild-type and Mutated MurB Proteins—Purified wild-type MurB was examined for UDP-GlcNAcEP reductase activity under aerobic conditions. NADPH oxidation by wild-type MurB was dependent on the concentrations of both UDP-GlcNAcEP and NADPH (Fig. 4, *A* and *B*, respectively). The K_m value for UDP-GlcNAcEP or NADPH was 53 or 4.1 μM, respectively, which is similar to that of *E. coli* MurB (14). Production of UDP-*N*-acetylmuramic acid in the reaction was confirmed by HPLC analysis with chemically characterized UDP-*N*-acetylmuramic acid as a standard (data not shown).

Next, we examined the ability of the mutant proteins to catalyze UDP-GlcNAcEP-dependent NADPH oxidation under anaerobic conditions, because the reoxidation of the reduced form of MurB is greatly reduced in the absence of oxygen. The wild-type MurB enhanced UDP-GlcNAcEP-dependent oxidation of NADPH, but the mutated forms of MurB lacked this increase (Fig. 5). Whereas the UDP-GlcNAcEP-dependent oxidation of NADPH by each mutated MurB protein was below the significant level, we could not deny the possibility that the background amount, that is the NADPH oxidation in the absence of UDP-GlcNAcEP, hid the small activities of any proteins to oxidize NADPH in a UDP-GlcNAcEP-dependent manner.

UDP-GlcNAcEP-independent Oxidation of NADPH by Mutated MurB Proteins—MurB catalyzes the two reaction steps; the first is the reduction of FAD by NADPH, and the second is the electron transfer from $FADH_2$ to UDP-GlcNAcEP (Fig. 1). Under aerobic conditions, one can examine the first half of the reaction, because the reduced MurB is reoxidized by molecular oxygen, allowing UDP-GlcNAcEP-independent NADPH oxidation to proceed (18, 25). Hence, we examined the activity of the mutated *S. aureus* MurB proteins under aerobic conditions. We found that all of the mutated MurB proteins catalyzed the oxidation of NADPH under aerobic conditions (Fig. 6). The K_m for NADPH was 38 μM for wild-type MurB and 3.3–36 μM for mutated proteins (Table 4), suggesting that the mutant MurB proteins do not show a loss of affinity for NADPH. Under these conditions, the rate of NADPH oxidation by the free form of FAD in the presence of 150 μM NADPH was 0.19 mmol/min/mol of FAD, which is much lower than the rates catalyzed by the mutant MurB proteins (Table 4).

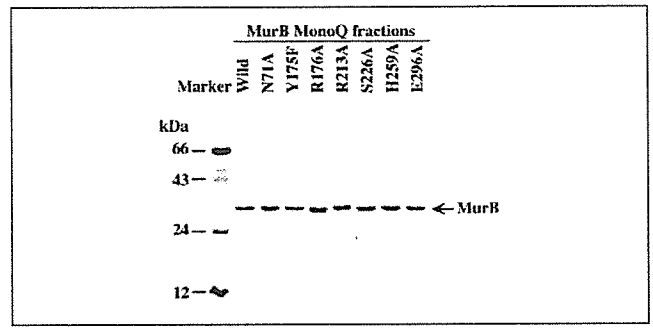

FIGURE 3. **Purified fraction of wild-type and mutant MurB.** Each MurB (Fraction IV; 2 μg) was analyzed by SDS-polyacrylamide (12.5%) gel electrophoresis and stained with CBB R-250.

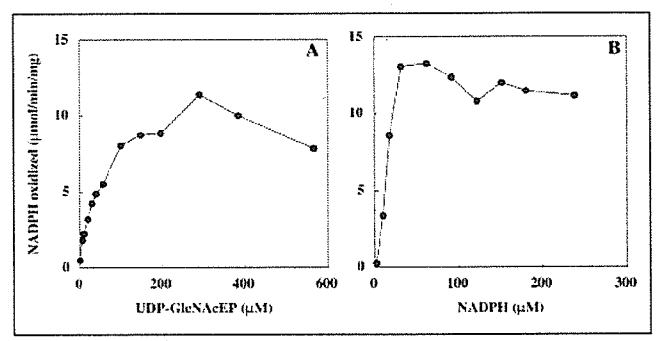

FIGURE 4. **UDP-GlcNAcEP reductase activity of *S. aureus* wild-type MurB.** The K_m for UDP-GlcNAcEP in the presence of 150 μM NADPH (*A*) and for NADPH in the presence of 100 μM UDP-GlcNAcEP (*B*) was determined under aerobic conditions using wild-type MurB. In both cases, the initial velocity for NADPH oxidation was determined. Results are representative of at least two independent experiments.

When NADPH reduces MurB-bound FAD to $FADH_2$, the yellow color of the oxidized form of MurB is immediately bleached (23). We also found that the yellow color of the oxidized form of the mutant and wild-type MurB protein was reduced by the addition of NADPH under both aerobic and anaerobic conditions (data not shown). These results indicated that the mutant MurB proteins can carry out the first catalytic step, namely the reduction of bound FAD by NADPH (Fig. 1).

UDP-GlcNAcEP Inhibition of NADPH Oxidation by the Mutant Enzymes—Both NADPH and UDP-GlcNAcEP have been shown to bind to the same site on MurB, which prevents them from binding at the same time (14). Consistent with this, UDP-GlcNAcEP had a biphasic

effect on the NADPH oxidation by the wild-type protein: stimulatory at low concentrations and inhibitory at high concentrations (Fig. 4*A*). Since UDP-GlcNAcEP failed to stimulate the NADPH oxidation by the mutant enzymes (Fig. 5), the mutations might affect the ability of UDP-GlcNAcEP to inhibit NADPH oxidation. To examine this point, we assayed the mutant enzymes under aerobic conditions. As under anaerobic conditions (Fig. 5), the mutant MurB proteins did not stimulate the oxidation of NADPH by UDP-GlcNAcEP under aerobic conditions (Fig. 7). In these experiments, UDP-GlcNAcEP inhibited NADPH oxidation by the N71A, Y175F, S226A, and E296A proteins; however, the inhibitory effect of UDP-GlcNAcEP on NADPH oxidation was much less for the R176A, R213A, and H259A proteins (Fig. 7). These results suggest that the former four mutant proteins have normal affinity for UDP-GlcNAcEP, whereas the later three have reduced affinity for this ligand. Additionally, the ability of UDP-GlcNAcEP to inhibit NADPH oxidation by the former four mutant proteins supports the idea that UDP-GlcNAcEP and NADPH share a binding pocket in *S. aureus* MurB.

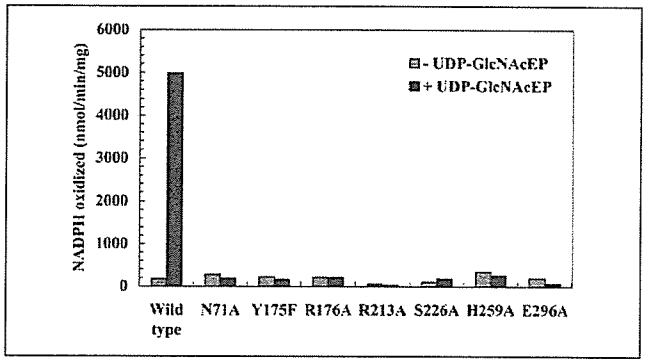

FIGURE 5. **Loss of UDP-GlcNAcEP reductase activity in mutant MurB proteins.** The initial velocity for NADPH oxidation by MurB proteins was determined in the presence (*black bar*) or absence (*gray bar*) of 100 μM UDP-GlcNAcEP under anaerobic conditions in a solution containing glucose oxidase, catalase, and glucose.

Absorption Spectrum Analyses for Mutated MurB Proteins—To determine whether the mutant proteins have altered abilities to bind FAD, we evaluated their FAD content and the absorption spectra for bound FAD. Flavin removed from the mutant or wild-type MurB proteins showed fluorescence peaks with the same retention time on HPLC as the FAD standard (data not shown). The amount of FAD in each MurB was determined to be 0.8–1.1 mol/mol of MurB, suggesting that each mutated MurB contains an equivalent amount of noncovalently bound FAD.

Next, the absorption spectra of FAD bound to wild-type and mutant MurB proteins were compared under aerobic conditions, wherein MurB is in an oxidized form. Wild-type MurB showed two characteristic absorption maximums for FAD, one of which was at 462 nm. Other than R213A, all of the mutant MurB proteins had an absorption maximum at 461 or 462 nm. R213A, in contrast, had an absorption maximum at 454 nm, which is noticeably different from the wild type. This result indicates that the electronic state of flavin is significantly different in the R213A and wild-type forms of MurB. In other words, Arg^{213} may help maintain the electronic state of FAD. This characteristic differentiates R213A from the other mutant MurB proteins.

Difference Spectrum Analysis for Interaction with NADP$^+$—Positively charged residues of MurB are thought to be involved in the interaction with $NADP^+$ (22). We next examined $NADP^+$ binding by the mutant MurB proteins by following the increase in absorbance at 510 nm upon $NADP^+$ binding (22). Difference spectrum for $NADP^+$ binding to wild-type MurB showed a characteristic peak at 510 nm under aerobic conditions (Fig. 8*C*). The extent of the increase in absorbance increase was dependent on the concentration of $NADP^+$ (Fig. 8*A*), which is consistent with the characteristics of *E. coli* MurB. The K_d value for $NADP^+$ for wild-type MurB was calculated to be 16 μM (Table 4). MurB mutants N71A, Y175F, R176A, S226A, and E296A had absorbance increases at 510 nm due to the addition of $NADP^+$ (Fig. 8*A*). There was less than a 5-fold difference in K_d values for these mutated forms MurB for $NADP^+$ compared with the wild-type enzyme (Table 4). Therefore, oxidized forms of the N71A, Y175F, R176A,

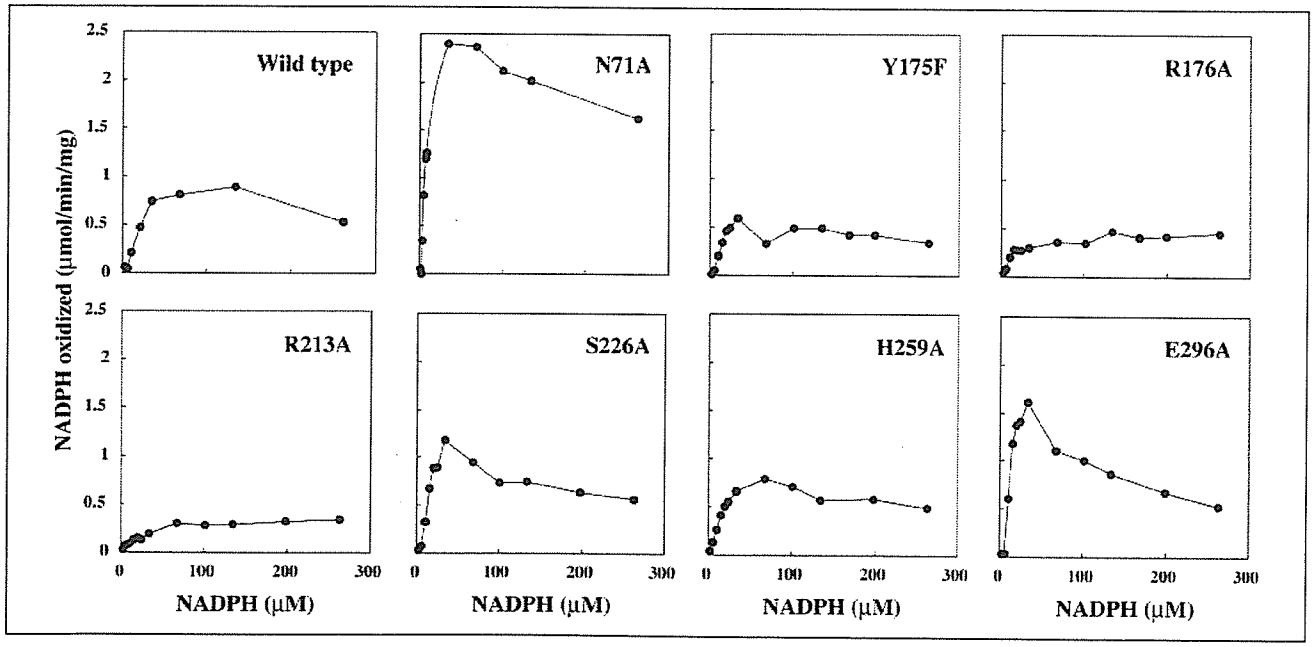

FIGURE 6. **UDP-GlcNAcEP-independent NADPH oxidation by wild-type and mutant MurB under aerobic conditions.** The initial velocity of NADPH oxidation by each MurB in the absence of UDP-GlcNAcEP was determined under aerobic conditions, wherein oxygen-mediated reoxidation of reduced MurB protein took place. The K_m and V_{max} values are summarized in Table 4.

TABLE 4
Kinetic constants for wild-type and mutated MurB proteins

MurB	K_m NADPH[a]	V_{max}[a]	V_{max}/K_m[a]	K_d $NADP^+$[b]	K_d UDP-GlcNAcEP[b]
	μM	*mol/min/mol MurB*	$\mu M^{-1}\ min^{-1}$	μM	μM
Wild type	38	40.5	1.0	16	41
N71A	8.0	91.8	11.4	20	12
Y175F	9.5	15.7	1.6	27	173
R176A	23	16.7	0.7	43	—[c]
R213A	36	13.3	0.3	—[c]	—[c]
S226A	3.3	34.8	10.5	73	180
H259A	24	36.8	1.5	—[c]	—[c]
E296A	14	77.5	5.5	40	9.4

[a] K_m, V_{max}, and V_{max}/K_m for the NADPH oxidase activity in the absence of UDP-GlcNAcEP under aerobic conditions have been calculated from Fig. 6.
[b] K_d values for $NADP^+$ and UDP-GlcNAcEP were calculated from Fig. 8.
[c] The K_d value could not be determined by a difference spectrum.

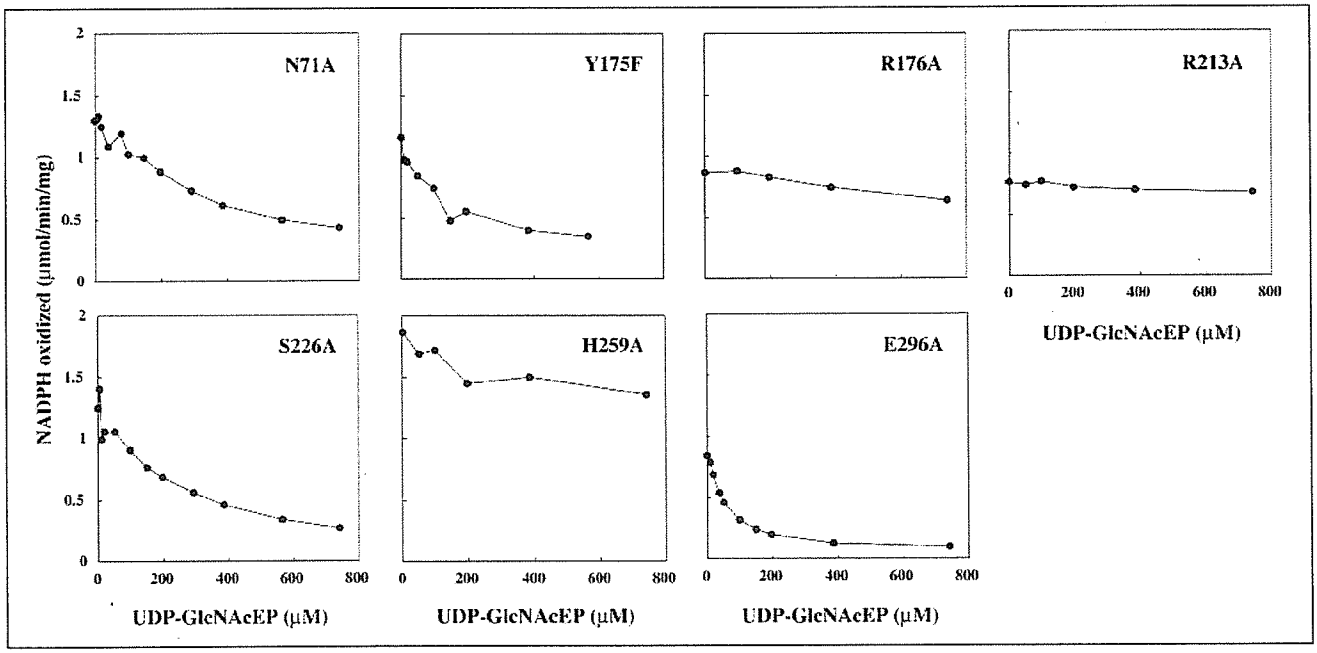

FIGURE 7. **Altered inhibitory mode of UDP-GlcNAcEP upon NADPH oxidation by the mutated forms of MurB.** The effect of UDP-GlcNAcEP on the initial velocity of NADPH oxidation by each MurB under aerobic conditions was determined as described in Fig. 6. In each case, the assay was carried out in the presence of 150 μM NADPH. Results are representative of more than two independent experiments.

S226A, and E296A mutants retain their affinity for $NADP^+$. Similarly, *E. coli* MurB S229A, which corresponds to *S. aureus* MurB S226A, was previously shown to have an affinity for $NADP^+$ that is comparable with wild-type MurB (18).

For H259A and R213A, the difference spectra due to the $NADP^+$ addition were significantly different from that of the wild-type enzyme (Fig. 8, *D* and *E*). These mutant MurB proteins did not show difference spectrum peaks at 510 nm (Fig. 8*A*). This suggests that these mutated MurBs have altered interactions between FAD and $NADP^+$; specifically, both His^{259} and Arg^{213} are required for proper changes in the electronic state of the oxidized form of the MurB upon interaction with $NADP^+$. Because the R213A mutant has a deficiency in the maintenance of the electronic state of FAD (see "Absorption Spectrum Analyses for Mutated MurB Proteins"), the absence of a difference spectrum peak at 510 nm with $NADP^+$ is probably due to a secondary effect.

Difference Spectrum Analysis for Interaction with UDP-GlcNAcEP—Next, we measured the difference spectra with UDP-GlcNAcEP for mutant MurB proteins under aerobic conditions. The difference spectrum for the wild-type protein with UDP-GlcNAcEP showed a peak at 510 nm (Fig. 8*F*). The height of this difference peak depended on the concentration of UDP-GlcNAcEP (Fig. 8*B*). The difference spectrum peak at 510 nm upon UDP-GlcNAcEP binding was also observed for N71A, Y175F, S226A, and E296A (Fig. 8*B*). The K_d values for UDP-GlcNAcEP of these mutated forms of MurB were within 5-fold of the wild-type value (Table 4), suggesting that these mutated MurBs retain their affinity for UDP-GlcNAcEP.

In contrast, the difference spectrum for the R176A, R213A, and H259A mutants with UDP-GlcNAcEP was significantly different from that of the wild type; these mutants did not show the characteristic peak at 510 nm found with the wild-type enzyme (Fig. 8, *G–I*). The results suggest that either R176A, R213A, and H259A lose the affinity for UDP-GlcNAcEP or they lose the ability to cause a spectrum change for the FAD cofactor upon binding of UDP-GlcNAcEP. The former possibility appears to agree with the results shown in Fig. 7, that NADPH oxidation by R176A, R213A, and H259A was poorly inhibited by UDP-GlcNAcEP under aerobic conditions. Again, for R213A, the secondary effect caused by a loss of the ability to maintain the electronic state of the FAD might explain the lack of a difference spectrum peak at 510 nm upon the addition of UDP-GlcNAcEP.

Identification of Four Groups of Active Site Essential Amino Acids—Based on absorption and difference spectrum analyses, we were able to

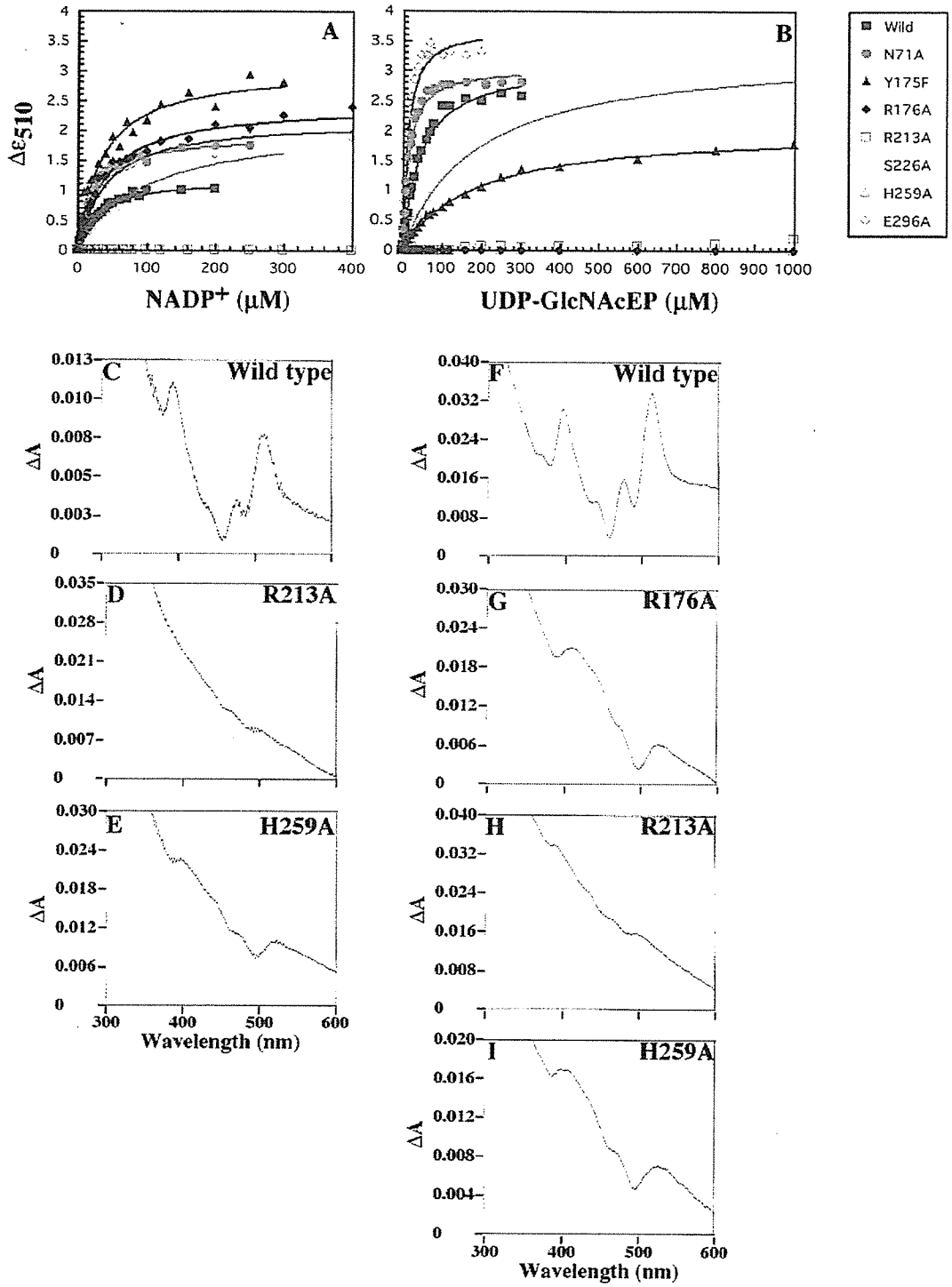

FIGURE 8. **Difference absorption spectra of the oxidative form wild-type and mutant MurB with NADP$^+$ or UDP-GlcNAcEP.** Enzymes were titrated under aerobic conditions, and the absorbance change at 510 nm as a function of NADP$^+$ (*A*) or UDP-GlcNAcEP (*B*) was plotted. Difference spectra, which were computed from the spectra in the presence and absence of 200 μM NADP$^+$ (*C–E*) or 200 μM UDP-GlcNAcEP (*F–I*), are shown for wild-type MurB (*C* and *F*), R176A (*G*), R213A (*D* and *H*), or H259A (*E* and *I*). The K_d values are summarized in Table 4.

separate the mutant MurB proteins into four categories. The first includes R213A. In this study, the absorption maximum at 462 nm for FAD in the wild-type MurB protein shifted to 454 nm in R213A. Furthermore, R213A did not show a characteristic increase at 510 nm in the difference spectrum upon binding either NADP$^+$ or UDP-GlcNAcEP. These results suggest that the electronic state of the isoalloxazine ring of FAD is disturbed in R213A. This means that Arg^{213} is important for maintaining the electronic state of the isoalloxazine ring of FAD, which